Numerical simulations of superconducting rings using a Ginzburg-Landau model

by

Marcus Calhoun-Lopez

A thesis submitted to the graduate faculty

in partial fulfillment of the requirements for the degree of

MASTER OF SCIENCE

Major: Applied Mathematics

Major Professors: Max Gunzburger and Janet Peterson

Iowa State University

Ames, Iowa

2001

Graduate College
Iowa State University

This is to certify that the Master's thesis of

Marcus Calhoun-Lopez

has met the thesis requirements of Iowa State University

Signatures have been redacted for privacy

TABLE OF CONTENTS

LIST OF TABLES

LIST OF FIGURES

1 INTRODUCTION

Early years of superconductivity

At temperatures near absolute zero, the properties of certain materials change, and they become superconductors. Type-I superconductors are characterized by the properties of perfect conductance, which is zero resistivity, and perfect diamagnetism, which is the exclusion of magnetic fields. Type-II superconductors behave like type-I superconductors at low magnetic fields, but at higher magnetic fields, they allow the partial penetration of the field at discrete areas called vortices. The Ginzburg-Landau (GL) model provides a mezoscale model for studying the behavior of both types of superconductors.

The perfect conductivity of superconductors was discovered by Heike Kamerlingh Onnes in 1911 [1, page 37]. Onnes was the first to find evidence of superconductivity and gave the phenomenon its name [1, page 37]. Scientists of the time already knew that resistance decreased with temperature, but in experiments with mercury and liquid helium, Onnes noticed that at a critical temperature (which is about $4.2°K$ for mercury), the resistivity dropped abruptly to zero [1, page 37].

The perfect conductance discovered by Onnes affects how a superconductor interacts with a magnetic field. According to classical electrodynamics, a perfect conductor would not allow the penetration of a magnetic field, and any field in the material as it is cooled below the critical temperature would be trapped within the material. In 1933, Walther Meissner and R. Ochsenfeld showed that superconductors not only exclude exterior magnetic fields, but also expel any magnetic field in the material [1, page 43]. The perfect diamagnetism of superconductors is also known as the Meissner effect.

In 1950, Vitaly L. Ginzburg and Lev Landau proposed a phenomenological theory based on phase transitions to explain superconductivity [2, page 248]. In the absence of applied magnetic fields, the phase transition between the normal and superconducting states is second-order. Landau had already developed a phenomenological theory of phase transitions based on the expansion of the free energy (which was assumed to be analytic) in powers of an order parameter [3, pages 39–41]. The GL model added to the free energy terms to allow for applied magnetic fields and a spatially varying order parameter [3, page 43]. Based on the success of the London equations, an earlier model of superconductivity,

the GL model also incorporated a complex order parameter, the square of whose magnitude is the order parameter from the original Landau theory of second order phase transitions [3, page 43]. The final result is a free energy that is real and gauge invariant. Minimizing the free energy with respect to the complex order parameter and magnetic potential gives the GL equations, which can be used to study superconductivity.

When first introduced, the GL model was slow to gain acceptance in the physics community [2, page 249]. L. P. Gor'kov, however, showed in 1958 that the GL equations, which were originally based on a phenomenological mezoscale model, can also be obtained as an approximation of the more accepted microscopic theory of superconductivity of John Bardeen, Leon Cooper, and Robert Schrieffer (BCS) [4, page 111]. Another triumph of the GL model came with the discovery of type-II superconductors. In 1957, Alexey A. Abrikosov showed that the GL equations model type-II superconductors, which had not yet been discovered when Ginzburg and Landau formulated their theory [2, pages 250–252]. So while slow to gain acceptance, the GL model has proven to be a useful tool in studying the phenomenon of superconductivity.

Applications of superconductivity

The potential for useful applications of superconductivity has been evident from the earliest days after its discovery. Onnes himself imagined that it would lead to wires capable of efficiently transporting electricity and to electromagnets capable of producing powerful magnetic fields [8, page 6]. The limitations of superconductivity, however, quickly became evident. It is expensive to produce the superconducting materials and to keep them at temperatures near absolute zero. Further, the superconducting state is easily destroyed by even modest magnetic fields and electric currents. So for decades after its discovery, few real world applications of superconductivity could be found. Starting in 1986, new materials were developed that greatly increased the maximum temperature at which the superconducting state could be maintained [8, pages 123–124]. The discovery of these high temperature superconductors has ushered in a new era of research into superconducting materials and their applications. The research has resulted in several large scale projects which incorporate superconducting materials with many more under consideration.

In theory, superconductors could enhance old technologies and create entirely new ones. Since they are perfect conductors, superconductors could be used to efficiently transport electricity. Resistivity can steal about 5% of the power transported by even the best normal cable [8, page 105]. Considering the amount of electricity used every day, this adds up to a huge waste of power. A superconducting wire

would virtually eliminate such waste and save a great deal of money. Zero resistance would also allow the production of strong magnetic fields. Such fields can be produced by running a strong electric current through a wire. If the wire has any resistance, a strong current will produce enough heat to destroy the wire. If a superconducting wire is used, no energy is lost due to resistivity and so much more powerful magnetic fields can be produced. Superconductors can also be used to create new technologies. When a thin layer of insulating material is placed between two superconducting regions, called a Josephson junction, a voltage across the junction abruptly appears at some current [8, page 98]. A new type of computer could be built by using Josephson junctions. A zero voltage could represent the binary digit `0`, while a non-zero voltage represents `1`. The current applied to the junction then controls its state. This new type of computer would process a signal much faster than conventional computers [8, page 120]. In theory, superconductors seem to hold limitless potential for new and improved technologies.

In practice, the superconducting state is often too difficult and expensive to maintain to be of practical use. Onnes discovered the superconductivity of mercury at the temperature of outer space [1, page 33]. Although other materials maintain the superconducting state at higher temperatures, the cost of the cryogenic systems required can easily offset any advantages in real world applications. At any temperature, superconductivity is lost in the presence of a magnetic field that is greater than some critical field. This limits the current that can pass through a superconducting wire since the magnetic field produced by a strong current will be greater than the critical field. So the applicability of superconductivity to the transport of electricity and the production of strong magnetic fields is limited. Even if the conditions for superconductivity were ideal, the production of materials capable of becoming superconductors is expensive. For many years after its discovery, the delicacy and expense of maintaining the superconducting state kept its potential for new and improved technologies from being fulfilled.

Hopes for practical applications of superconductivity surged again with the discovery of new high temperature superconductors by George Bednorz and Alex Müller in 1986 and by Paul Chu and Maw-Kuen Wu in 1987 [8, page 123]. From 1973–1986, the highest known critical temperature was $23°K$ [8, page 124]. The record was shattered in 1986 with $30°K$ and again in 1987 with $90°K$ [8, page 124]. With these discoveries came a renewed interest in superconductivity that continues today.

Researchers are continually developing new and better superconductors. Lucent Technologies recently announced a new type of buckyball, a crystal made of carbon molecules, that has the potential to remain superconducting at higher temperatures [9]. Researchers led by Dr. Jun Akimitsu found that the common metallic compound magnesium boride is a superconductor [10]. The discovery is significant

because the compound is cheaper than most other superconductors. Bell Labs has even announced the discovery of a plastic superconductor, which is relatively cheap and malleable [11]. Such better and cheaper superconductors make it feasible to develop technologies based on superconductivity.

Many devices now incorporate superconductors, with more in development. Superconductors are used in Magnetic Resonance Imaging (MRI), an invaluable diagnostic tool used in hospitals [8, page 111]. A high speed levitation train in Japan uses superconducting magnets [8, page 115]. More recently, the Wisconsin Public Service Corporation began using superconducting magnets in several of its energy storage units [12]. American Superconductor and Litton Industries will use superconducting wires in the electric motors of some of their ships [13]. At Los Alamos Lab, the quantum computers, a new type of computer still in development, use superconducting magnets to manipulate atoms [14]. Quantum computers, which are radically different from current computers, promise to deliver computation speeds which are impossible to attain using conventional technology. So superconductivity has begun to yield important technological advances.

When superconductivity was discovered in 1911, there seemed to be no limit to its usefulness. After ninety years of research, superconductors are finally beginning to live up to their potential.

Outline of presentation

In this thesis, we present numerical simulations of a type-II superconducting ring using the Ginzburg-Landau model of superconductivity. In Chapter 2, we present the time dependent Ginzburg-Landau model of superconductivity. In Chapter 3, we present a weak formulation of the equations on an annulus domain. The weak form is the problem we approximate to obtain our simulations. To dicretize the problem, we use a Galerkin finite element method in space and the backward Euler method in time. The finite dimensional approximation of the weak solution is presented in Chapter 4. Finally, we report the numerical results of our experiments in Chapter 5. Our numerical simulation yields a complex order parameter $\psi = |\psi| e^{i\phi}$. $|\psi|^2$ is the density of superconducting charge carriers. By generating contour plots of $|\psi|^2$ and vector plots of ϕ, we are be able to determine the behavior of the vortices as we vary the applied magnetic field and inner radius of the ring. The motion of a vortex induces resistance in a superconductor [15, page 41], so understanding and controlling vortex behavior is important in the construction of devices that use superconductors.

Literature review

A historical overview of superconductivity can be found in [1], [2], and [8]. Rigourous developments of mezoscale models and properties of superconductors can be found in [3], [4], and [20]. A less rigourous book that still provides an overview of the important properties of superconductors is [15]. The development of the time dependent Ginzburg-Landau model of superconductivity can be found in [5]. A mathematical treatment of the Ginzburg-Landau model, including results using the finite element method, is located in [16] and [17]. Simulations of type-II superconductors using the Ginzburg-Landau model and the finite element method can be found in [21]. An alternative method of solving the GL model on an annulus domain is located in [6].

2 GINZBURG-LANDAU MODEL

Time-dependent Ginzburg-Landau equations and boundary conditions

Let $\Omega \subseteq \mathbb{R}^n$ with $n \in \{1,2,3\}$ be the region occupied by a superconducting material, and let $\Omega_e = \mathbb{R}^n \backslash \Omega$. The GL model gives the Gibbs free energy, $\mathcal{G}$, of the system as

$$\begin{aligned} \mathcal{G}(\psi, \mathbf{A}) &= \int_\Omega \left[f_n + \alpha |\psi|^2 + \frac{\beta}{2} |\psi|^4 + \frac{1}{2m_s} \left| \left(i\hbar \nabla + \frac{e_s}{c} \mathbf{A} \right) \psi \right|^2 + \frac{|\mathbf{h}|^2}{8\pi} - \frac{\mathbf{h} \cdot \mathbf{H}}{4\pi} \right] d\Omega \\ &\quad + \int_{\Omega_e} \left[f_e + \frac{|\mathbf{h}|^2}{8\pi} - \frac{\mathbf{h} \cdot \mathbf{H}}{4\pi} \right] d\Omega_e, \end{aligned} \tag{2.1}$$

where we define the variables in Table 2.1.

Table 2.1 List of variables

$\mathcal{G}$	Gibbs free energy	e_s, m_s	charge and mass respectively of superconducting charge carriers
t	time		
$\mathbf{r}$	position	ν	conductance of normal material
f_n, f_e	free energy densities of normal materials in Ω and Ω_e respectively when $\mathbf{h} \equiv \mathbf{0}$	α, β	temperature dependent parameters which characterize a material
$\psi(\mathbf{r})$	complex order parameter	c	speed of light in a vacuum
n_s	real parameter in the GL model; density of superconducting charge carriers $\left(= \lvert\psi\rvert^2\right)$	γ	a constant time relaxation parameter
		$2\pi\hbar$	Plank's constant
		i	$\sqrt{-1}$
$\mathbf{A}$	magnetic potential	λ	penetration depth
$\mathbf{h}$	magnetic field $(= \nabla \times \mathbf{A})$	ξ	coherence length
$\mathbf{H}$	applied magnetic field	κ	Ginzburg-Landau parameter $(= \lambda/\xi)$
Φ	electric potential		
$\mathbf{E}$	electric field		
$\mathbf{J}$	current density		

According to the BCS theory, the superconducting charge carriers are pairs of electrons called Cooper pairs [4, page 44]. The mass and charge of these pseudoparticles are then twice those of an electron.

α and β are parameters that depend only on the temperature and the material. β is always positive, but α is positive only in the normal state and negative in the superconducting state.

Near the intersection of superconducting and normal regions, Cooper pairs form in the normal region, and the density of pairs is reduced in the superconducting region. Collectively, these two phenomena are known as the proximity effect [6, page 97–99]. We choose a normal region such that neither of these effects occur. A vacuum is the simplest example of such a normal region.

The GL theory postulates that the system will go to a state where $\mathcal{G}$ is minimized. Using standard techniques from the calculus of variations, we can obtain the equations and boundary conditions for the steady state of the system.

A model for the intermediate states of the system can be found in Gor'kov and Kopnin [5]. The time dependent Ginzburg-Landau (TDGL) equations are

$$\gamma\left(\hbar\frac{\partial\psi}{\partial t}+ie_s\Phi\psi\right)+\frac{1}{2m_s}\left(i\hbar\boldsymbol{\nabla}+\frac{e_s}{c}\mathbf{A}\right)^2\psi+\alpha\psi+\beta\left|\psi\right|^2\psi=0 \text{ in } \Omega \text{ and} \tag{2.2}$$

$$\nu\left(\frac{1}{c}\frac{\partial\mathbf{A}}{\partial t}+\boldsymbol{\nabla}\Phi\right)+\frac{c}{4\pi}\boldsymbol{\nabla}\times\boldsymbol{\nabla}\times\mathbf{A}+\frac{ie_s\hbar}{2m_s}\left(\psi^*\boldsymbol{\nabla}\psi-\psi\boldsymbol{\nabla}\psi^*\right)+\frac{{e_s}^2}{m_sc}\left|\psi\right|^2\mathbf{A}=\frac{c}{4\pi}\boldsymbol{\nabla}\times\mathbf{H} \text{ in } \Omega. \tag{2.3}$$

The boundary conditions are

$$\left(i\hbar\boldsymbol{\nabla}\psi+\frac{e_s}{c}\mathbf{A}\psi\right)\cdot\hat{\mathbf{n}}=0 \text{ on } \Gamma, \tag{2.4}$$

$$\left[(\boldsymbol{\nabla}\times\mathbf{A}-\mathbf{H})\times\hat{\mathbf{n}}\right]=\mathbf{0} \text{ on } \Gamma, \text{ and} \tag{2.5}$$

$$\left[\mathbf{A}\times\hat{\mathbf{n}}\right]=\mathbf{0} \text{ on } \Gamma, \tag{2.6}$$

where Γ is the boundary of Ω, ψ^* is the complex conjugate of ψ, $\hat{n}$ is the unit normal vector, and $[\cdot]$ is the jump across Γ.

Since we have assumed that $|\psi|=0$ in Ω_e, we can couple the TDGL equations with the normal equations of electrodynamics. We use the quasi-static field approximation [7, page 218–219] in which we ignore Maxwell's correction to Faraday's law and hence have:

$$\begin{aligned}
\boldsymbol{\nabla}\times(\mathbf{h}-\mathbf{H}) &= \frac{4\pi}{c}\mathbf{J} \text{ (Faraday's Law)},\\
\mathbf{J} &= \nu\mathbf{E} \text{ (Ohm's Law)},\\
\mathbf{E} &= -\boldsymbol{\nabla}\Phi-\frac{1}{c}\frac{\partial\mathbf{A}}{\partial t} \text{ (potential representation of } \mathbf{E}), \text{ and}\\
\mathbf{h} &= \boldsymbol{\nabla}\times\mathbf{A} \text{ (potential representation of } \mathbf{h}).
\end{aligned}$$

So we couple equations (2.2)–(2.3) with

$$\nu\left(\frac{1}{c}\frac{\partial\mathbf{A}}{\partial t}+\boldsymbol{\nabla}\Phi\right)+\frac{c}{4\pi}\boldsymbol{\nabla}\times\boldsymbol{\nabla}\times\mathbf{A}=\frac{c}{4\pi}\boldsymbol{\nabla}\times\mathbf{H} \text{ in } \Omega_e. \tag{2.7}$$

At sufficiently large distances, the effect of the superconducting material on the magnetic field should be negligible. We therefore have the additional boundary condition

$$\mathbf{h}=\boldsymbol{\nabla}\times\mathbf{A}\rightarrow\mathbf{H} \text{ as } |\mathbf{r}|\rightarrow\infty. \tag{2.8}$$

Dimensionless TDGL equations and boundary conditions

All equations in the previous section were in Gaussian units. The TDGL equations and boundary conditions will be simpler to work with if we use a dimensionless system. The important scales for a superconducting material are the penetration depth, λ, the coherence length, ξ, and the critical field for type-I superconductors, H_c. As discussed in Chapter 1, superconducting materials expel magnetic fields. λ measures the exponential rate at which the magnetic field penetrates the superconducting sample [4, page 5]. As we can see from equation 2.1, $\mathcal{G}$ increases as $|\nabla\psi|$ increases, so variations in ψ penalize the energy. For type-II superconductors, no variations would penalize the energy even more. ξ is a measure of the distance ψ can vary while still minimizing $\mathcal{G}$ [4, page 11]. H_c is the theoretical limit of the magnetic field above which a type-I superconductor would become normal.

Table 2.2 Nondimensionalization of variables

t	$\rightarrow$	$t\frac{\gamma\hbar}{\lvert\alpha\rvert}$	f_n	$\rightarrow$	$f_n\frac{\alpha^2}{\beta}$	H_c	$=$	$\sqrt{\frac{4\pi\alpha^2}{\beta}}$
$\mathbf{r}$	$\rightarrow$	$\mathbf{r}\ell$	f_e	$\rightarrow$	$f_e\frac{\alpha^2}{\beta}$	$\mathbf{H}$	$\rightarrow$	$\mathbf{H}H_c\sqrt{2}$
$\mathcal{G}$	$\rightarrow$	$\mathcal{G}\frac{\alpha^2\ell^n}{\beta}$	Φ	$\rightarrow$	$\Phi\frac{\lvert\alpha\rvert}{\gamma e_s}$	λ	$=$	$\sqrt{\frac{\beta m_s c^2}{4\pi\lvert\alpha\rvert{e_s}^2}}$
ψ	$\rightarrow$	$\psi\sqrt{\frac{\lvert\alpha\rvert}{\beta}}$	$\mathbf{J}$	$\rightarrow$	$\mathbf{J}\frac{cH_c}{\pi\ell\sqrt{8}}$	ξ	$=$	$\sqrt{\frac{\hbar^2}{2m_s\lvert\alpha\rvert}}$
$\mathbf{A}$	$\rightarrow$	$\mathbf{A}\ell H_c\sqrt{2}$	σ	$=$	$\frac{\nu\beta m_s}{\gamma{e_s}^2\hbar}$	ℓ	$\in$	$\{\xi,\lambda\}$

We translate our variables to dimensionless quantities using Table 2.2. In our new system of units, the Gibbs free energy is

$$\begin{aligned}\mathcal{G}(\psi,\mathbf{A}) &= \int_\Omega \left[f_n - |\psi|^2 + \frac{1}{2}|\psi|^4 + \left|\left(i\frac{\xi}{\ell}\nabla + \frac{\ell}{\lambda}\mathbf{A}\right)\psi\right|^2 + |\nabla\times\mathbf{A}|^2 - 2(\nabla\times\mathbf{A})\cdot\mathbf{H}\right] d\Omega \\ &\quad + \int_{\Omega_e}\left[f_e + |\nabla\times\mathbf{A}|^2 - 2(\nabla\times\mathbf{A})\cdot\mathbf{H}\right] d\Omega_e. \end{aligned} \tag{2.9}$$

The time dependent Ginzburg-Landau equations become

$$\frac{\partial\psi}{\partial t} + i\Phi\psi - \psi + |\psi|^2\psi + \left(i\frac{\xi}{\ell}\nabla + \frac{\ell}{\lambda}\mathbf{A}\right)^2\psi = 0 \text{ in } \Omega, \tag{2.10}$$

$$\sigma\left(\frac{\ell^2}{\lambda^2}\frac{\partial\mathbf{A}}{\partial t} + \frac{\xi}{\lambda}\nabla\Phi\right) + \nabla\times\nabla\times\mathbf{A} + \frac{i}{2}\frac{\xi}{\lambda}(\psi^*\nabla\psi - \psi\nabla\psi^*) + \frac{\ell^2}{\lambda^2}|\psi|^2\mathbf{A} = \nabla\times\mathbf{H} \text{ in } \Omega, \text{ and} \tag{2.11}$$

$$\sigma\left(\frac{\ell^2}{\lambda^2}\frac{\partial\mathbf{A}}{\partial t} + \frac{\xi}{\lambda}\nabla\Phi\right) + \nabla\times\nabla\times\mathbf{A} = \nabla\times\mathbf{H} \text{ in } \Omega_e. \tag{2.12}$$

The boundary conditions are

$$\left(i\frac{\xi}{\ell}\boldsymbol{\nabla}\psi + \frac{\ell}{\lambda}\mathbf{A}\psi\right)\cdot\hat{\mathbf{n}} = 0 \text{ on } \Gamma, \tag{2.13}$$

$$[(\boldsymbol{\nabla}\times\mathbf{A} - \mathbf{H})\times\hat{\mathbf{n}}] = 0 \text{ on } \Gamma, \tag{2.14}$$

$$[\mathbf{A}\times\hat{\mathbf{n}}] = 0 \text{ on } \Gamma, \text{ and} \tag{2.15}$$

$$\boldsymbol{\nabla}\times\mathbf{A} \to \mathbf{H} \text{ as } |\mathbf{r}| \to \infty. \tag{2.16}$$

We also have the initial conditions

$$\psi(\mathbf{x}, 0) = \psi_0(\mathbf{x}) \text{ in } \Omega \text{ and} \tag{2.17}$$

$$\mathbf{A}(\mathbf{x}, 0) = \mathbf{A}_0(\mathbf{x}) \text{ in } \Omega, \tag{2.18}$$

where $|\psi_0| \leq 1$ almost everywhere.

As we shall see in the next section, we can eliminate Φ from equations (2.10)–(2.12). It is then evident that for the steady state of the system (when $\frac{\partial\mathbf{A}}{\partial t} = \mathbf{0}$ and $\frac{\partial\psi}{\partial t} = 0$), $\mathbf{H}$ and $\kappa = \frac{\lambda}{\xi}$ completely determine the solution of the GL equations. κ also determines the type of superconductor that is being modeled. For type-I superconductors, $\kappa < 1/\sqrt{2}$. For type-II superconductors, $\kappa > 1/\sqrt{2}$.

Making TDGL equations well-posed

Given a solution of the TDGL equations, $(\psi, \mathbf{A}, \Phi)$, and function χ, then

$$\left(\psi e^{i\kappa\chi}, \mathbf{A} + \frac{\lambda^2}{\ell^2}\boldsymbol{\nabla}\chi, \Phi - \kappa\frac{\partial\chi}{\partial t}\right)$$

is also a solution. Such an ambiguity in the solution means that the equations are gauge invariant. From a physical standpoint, this is a strength of the model, but we must ensure that there is a unique solution to the equations. Requiring extra conditions on $(\psi, \mathbf{A}, \Phi)$ to remove the ambiguity is called fixing the gauge. After a gauge is chosen, the TDGL equations have a unique solution, and the solution is continuously dependent on the initial data [17].

For our numerical simulations, we choose the zero electric potential gauge, in which $\Phi = 0$ in $\mathbb{R}^n$, $\mathbf{A}\cdot\hat{\mathbf{n}} = 0$ on Γ, $\boldsymbol{\nabla}\cdot\mathbf{A} = 0$ in $\mathbb{R}^n$ at $t = 0$, and $\boldsymbol{\nabla}(\boldsymbol{\nabla}\cdot\mathbf{A}) = \mathbf{0}$ in $\mathbb{R}^n$.

3 WEAK FORMULATION OF TDGL EQUATIONS ON AN ANNULUS

Annulus superconducting region

Superconducting wires have important practical applications, but approximating the Ginzburg-Landau equations in three dimensions is computationally expensive. If the wire is infinitely long, then by symmetry, any ring cross-section behaves as a two dimensional annulus. Our simulations are over very small distances, so approximating the length of the wire to be infinitely long is reasonable since the length of the wire is much larger than the radius. To simulate a long superconducting wire, we approximate solutions of the TDGL equations on an annulus domain.

Let us now consider Ω to be a ring of inner radius R_1 and outer radius R_2 (so $n = 2$). Ω_e is split into two distinct regions Ω_0 and Ω_2, where

$$\begin{aligned} \Omega_0 &= \left\{\mathbf{r} \in \mathbb{R}^2 : |\mathbf{r}| < R_1\right\} \\ \Omega_2 &= \left\{\mathbf{r} \in \mathbb{R}^2 : |\mathbf{r}| > R_2\right\} \\ \Omega_e &= \Omega_0 \cup \Omega_2. \end{aligned}$$

Γ is partitioned into a circle of radius R_1, denoted by Γ_1, and a circle of radius R_2, denoted by Γ_2. A picture of the domain is given in Figure 3.1.

In order to ignore the proximity effect, we chose the normal material to be a vacuum. Since there are no charged particles to carry a current, $\nu = 0$ in Ω_e, where ν is the conductance. The applied magnetic field is taken to be perpendicular to the ring and uniform in space. Consequently, $\boldsymbol{\nabla} \times \mathbf{H} = \mathbf{0}$. Equation (2.12) now reduces to

$$\boldsymbol{\nabla} \times \mathbf{h} = \mathbf{0} \text{ in } \Omega_e.$$

We use an orthogonal Cartesian coordinate system to describe the system. Our superconducting ring is in the x-y plane with its center at the origin. The positive z-axis is taken to be in the direction of the applied magnetic field ($\mathbf{H} = |\mathbf{H}|\,\hat{z}$).

Since the ring is two dimensional, the vector $\mathbf{A}$ can not depend on z and does not have a component

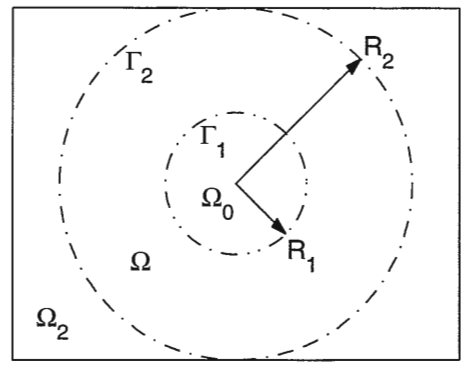

Figure 3.1 Annulus domain

in the z-direction.

$$\begin{aligned}
\mathbf{A} = A_x(x,y)\,\hat{x} + A_y(x,y)\,\hat{y} \quad &\Rightarrow \quad \mathbf{h} = h(x,y)\,\hat{z} \;\; (\mathbf{h} = \boldsymbol{\nabla} \times \mathbf{A}) \\
&\Rightarrow \quad \boldsymbol{\nabla} \times \mathbf{h} = \frac{\partial h}{\partial y}\hat{x} - \frac{\partial h}{\partial x}\hat{y} \\
&\Rightarrow \quad \mathbf{h} \text{ is constant in } \Omega_e \;\; (\boldsymbol{\nabla} \times \mathbf{h} = \mathbf{0}).
\end{aligned}$$

The boundary condition (2.16) tells us that $\mathbf{h} = \mathbf{H}$ in Ω_2.

With our choices of gauge, normal materials, and applied fields, equations (2.10)–(2.16) become:

$$\frac{\partial \psi}{\partial t} - \psi + |\psi|^2 \psi + \left(i\frac{\xi}{\ell}\boldsymbol{\nabla} + \frac{\ell}{\lambda}\mathbf{A} \right)^2 \psi = 0 \text{ in } \Omega, \tag{3.1}$$

$$\sigma\frac{\ell^2}{\lambda^2}\frac{\partial \mathbf{A}}{\partial t} + \boldsymbol{\nabla} \times \boldsymbol{\nabla} \times \mathbf{A} + \frac{i}{2}\frac{\xi}{\lambda}(\psi^*\boldsymbol{\nabla}\psi - \psi\boldsymbol{\nabla}\psi^*) + \frac{\ell^2}{\lambda^2}|\psi|^2\mathbf{A} - \boldsymbol{\nabla}(\boldsymbol{\nabla}\cdot\mathbf{A}) = \boldsymbol{\nabla} \times \mathbf{H} \text{ in } \Omega, \tag{3.2}$$

$$\boldsymbol{\nabla} \times \mathbf{A} - \mathbf{H} = \mathbf{0} \text{ in } \Omega_2, \tag{3.3}$$

$$\boldsymbol{\nabla} \times \mathbf{A} - \mathbf{H} \text{ is constant in } \Omega_0, \tag{3.4}$$

$$(\boldsymbol{\nabla}\psi)\cdot\hat{\mathbf{n}} = 0 \text{ on } \Gamma, \tag{3.5}$$

$$\mathbf{A}\cdot\hat{\mathbf{n}} = 0 \text{ on } \Gamma, \tag{3.6}$$

$$(\boldsymbol{\nabla} \times \mathbf{A} - \mathbf{H}) \times \hat{\mathbf{n}} = \mathbf{0} \text{ on } \Gamma_2, \tag{3.7}$$

$$[(\boldsymbol{\nabla} \times \mathbf{A} - \mathbf{H}) \times \hat{\mathbf{n}}] = \mathbf{0} \text{ on } \Gamma_1, \text{ and} \tag{3.8}$$

$$[\mathbf{A} \times \hat{\mathbf{n}}] = \mathbf{0} \text{ on } \Gamma. \tag{3.9}$$

Equations (3.1)–(3.9) are the version of the Ginzburg-Landau model we will use for our simulations.

Weak form of TDGL equations

One of our numerical techniques, the finite element method, requires us to approximate solutions to a weak formulation of the TDGL equations. The solution of the weak problem will be sufficiently smooth so it coincides with the classical solution.

To formulate the weak problem, let us present several standard definitions. Let α be an n-tuple of non-negative integers $\{\alpha_j\}_{j=1}^n$. We define $|\alpha| = \alpha_1 + \cdots + \alpha_n$. D^α is the differential operator

$$D^\alpha = \frac{\partial^{|\alpha|}}{\partial x_1^{\alpha_1} \cdots \partial x_n^{\alpha_n}},$$

where the derivatives are in the distributional sense. $L^2(\Omega)$ is the space of real square integrable functions on Ω. $\mathcal{L}^2(\Omega)$ is the space of complex square integrable functions on Ω. For non-negative integer m,

$$\begin{aligned}
H^m(\Omega) &= \left\{u \in L^2(\Omega) : D^\alpha u \in L^2(\Omega) \text{ for } 0 \le |\alpha| \le m\right\}, \\
\mathcal{H}^m(\Omega) &= \left\{u \in \mathcal{L}^2(\Omega) : D^\alpha u \in \mathcal{L}^2(\Omega) \text{ for } 0 \le |\alpha| \le m\right\}, \\
\mathbf{H}^m(\Omega) &= \left[H^m(\Omega)\right]^n \\
&= \left\{\mathbf{u} : u_j \in H^m(\Omega)\ \forall\ j \in \{1, 2, \ldots, n\}\right\}, \text{ and} \\
\mathbf{H}_n^m(\Omega) &= \left\{\mathbf{u} \in \mathbf{H}^m(\Omega) : \mathbf{u} \cdot \hat{\mathbf{n}} = 0 \text{ on } \Gamma\right\}.
\end{aligned}$$

$H^m(\Omega)$ and $\mathcal{H}^m(\Omega)$ are Banach spaces with the norm

$$\| u \|_m = \left(\sum_{|\alpha| \le m} \int_\Omega |D^\alpha u|^2 \, d\Omega \right)^{\frac{1}{2}}.$$

$\mathbf{H}^m(\Omega)$ and $\mathbf{H}_n^m(\Omega)$ are also Banach spaces with norm

$$\| \mathbf{u} \|_m = \left(\sum_{j=1}^n \| u_j \|_m^2 \right)^{\frac{1}{2}}.$$

We must also define spaces to account for the time dependence of the problem. For $T > 0$ and Banach spaces $B_r(\Omega)$ and $B_t(0,T)$,

$$B_t(0,T; B_r(\Omega)) = \left\{f : f(\cdot,t) \in B_r(\Omega) \text{ a.e. } t \in (0,T) \text{ and } \| f(\cdot,t) \|_{B_r(\Omega)} \in B_t(0,T)\right\}.$$

The spaces of functions we will consider are $\mathcal{V}(\Omega)$ and $\mathbf{V}(\Omega)$, where

$$\mathcal{V}(\Omega) = \mathcal{L}^\infty\left(0,T; \mathcal{H}^1(\Omega)\right) \cap \mathcal{H}^1\left(0,T; \mathcal{L}^2(\Omega)\right), \text{ and}$$

$$\mathbf{V}(\Omega) = \mathbf{L}^\infty\left(0,T; \mathbf{H}_n^1(\Omega)\right) \cap \mathbf{H}^1\left(0,T; \mathbf{L}^2(\Omega)\right).$$

We can now state the weak formulation of the TDGL equations: seek $\psi \in \mathcal{V}(\Omega)$ and $\mathbf{A} \in \mathbf{V}(\Omega) \cap \mathbf{V}(\Omega_0)$ such that

$$\int_\Omega \left\{ \frac{\partial \psi}{\partial t}\tilde{\psi} - \psi\tilde{\psi} + |\psi|^2 \psi\tilde{\psi} + \left[\left(i\frac{\xi}{\ell}\boldsymbol{\nabla} + \frac{\ell}{\lambda}\mathbf{A}\right)\psi\right] \cdot \left[\left(-i\frac{\xi}{\ell}\boldsymbol{\nabla} + \frac{\ell}{\lambda}\mathbf{A}\right)\tilde{\psi}\right] \right\} d\Omega = 0 \;\forall\; \tilde{\psi} \in \mathcal{H}^1(\Omega) \text{ and} \tag{3.10}$$

$$\begin{aligned}
&\int_\Omega \left[\frac{i}{2}\frac{\xi}{\lambda}\left(\psi^*\boldsymbol{\nabla}\psi - \psi\boldsymbol{\nabla}\psi^*\right)\cdot\tilde{\mathbf{A}} + \frac{\ell^2}{\lambda^2}|\psi|^2\,\mathbf{A}\cdot\tilde{\mathbf{A}}\right] d\Omega \\
&+ \int_\Omega \left[\sigma\frac{\ell^2}{\lambda^2}\frac{\partial \mathbf{A}}{\partial t}\cdot\tilde{\mathbf{A}} + (\boldsymbol{\nabla}\times\mathbf{A})\cdot\left(\boldsymbol{\nabla}\times\tilde{\mathbf{A}}\right) + (\boldsymbol{\nabla}\cdot\mathbf{A})\left(\boldsymbol{\nabla}\cdot\tilde{\mathbf{A}}\right) - \mathbf{H}\cdot\left(\boldsymbol{\nabla}\times\tilde{\mathbf{A}}\right)\right] d\Omega \\
&+ \int_{\Omega_0} \left[(\boldsymbol{\nabla}\times\mathbf{A})\cdot\left(\boldsymbol{\nabla}\times\tilde{\mathbf{A}}\right) - \mathbf{H}\cdot\left(\boldsymbol{\nabla}\times\tilde{\mathbf{A}}\right)\right] d\Omega_0 \\
&- \int_\Gamma \left[(\boldsymbol{\nabla}\cdot\mathbf{A})\left(\tilde{\mathbf{A}}\cdot\hat{\mathbf{n}}\right)\right] d\Gamma = 0 \;\forall\; \tilde{\mathbf{A}} \in \mathbf{H^1}(\boldsymbol{\Omega}) \cap \mathbf{H^1}(\boldsymbol{\Omega_0}).
\end{aligned} \tag{3.11}$$

The weak problem has a unique solution which is smooth enough to solve equations (3.1)–(3.9), the original strong formulation [17].

We can simplify the weak formulation by simplifying the integral over Ω_0. The fact that $\boldsymbol{\nabla}\times\mathbf{A}$ and $\mathbf{H}$ are constant in Ω_0 allows us to write:

$$\begin{aligned}
\int_{\Omega_0} \left[(\boldsymbol{\nabla}\times\mathbf{A} - \mathbf{H})\cdot\left(\boldsymbol{\nabla}\times\tilde{\mathbf{A}}\right)\right] d\Omega_0 &= (\boldsymbol{\nabla}\times\mathbf{A} - \mathbf{H})\cdot\left[\int_{\Omega_0}\left(\boldsymbol{\nabla}\times\tilde{\mathbf{A}}\right) d\Omega_0\right] \\
&= \left[\frac{1}{|\Omega_0|}\int_{\Omega_0}(\boldsymbol{\nabla}\times\mathbf{A})\, d\Omega_0 - \mathbf{H}\right]\cdot\left[\int_{\Omega_0}\left(\boldsymbol{\nabla}\times\tilde{\mathbf{A}}\right) d\Omega_0\right] \\
&= \left[\frac{1}{|\Omega_0|}\int_{\Gamma_1}(\mathbf{A}\times\hat{\mathbf{n}})\, d\Gamma_1 - \mathbf{H}\right]\cdot\left[\int_{\Gamma_1}\left(\tilde{\mathbf{A}}\times\hat{\mathbf{n}}\right) d\Gamma_1\right],
\end{aligned}$$

where $|\Omega_0|$ is the area of Ω_0.

The boundary condition $\mathbf{A}\cdot\hat{\mathbf{n}} = 0$ on Γ is, as we shall see in the next section, a hindrance to numerical computation for a curved domain. We therefore alter it slightly to $\mathbf{A}\cdot\hat{\mathbf{n}} + \epsilon\boldsymbol{\nabla}\cdot\mathbf{A} = 0$ on Γ, where $\epsilon > 0$ is the penalty parameter. The extra term is also incorporated into the definition of $\mathbf{V}(\Omega)$. For small ϵ, our modified boundary condition is a good approximation of the original. By rewriting the condition as $\boldsymbol{\nabla}\cdot\mathbf{A} = -\frac{1}{\epsilon}\mathbf{A}\cdot\hat{\mathbf{n}}$, we can substitute $\boldsymbol{\nabla}\cdot\mathbf{A}$ into the line integral in equation (3.11). With a careful choice of ϵ, the error induced by the modification will be of the same order magnitude as the error of our numerical method [18].

Our weak formulation becomes: seek $\psi \in \mathcal{V}(\Omega)$ and $\mathbf{A} \in \mathbf{V}(\Omega)$ such that

$$\int_\Omega \left\{ \frac{\partial \psi}{\partial t}\tilde{\psi} + \left(\frac{\xi}{\ell}\right)^2 (\boldsymbol{\nabla}\psi)\cdot(\boldsymbol{\nabla}\tilde{\psi}) + i\frac{\xi}{\lambda}\mathbf{A}\cdot\left(\tilde{\psi}\boldsymbol{\nabla}\psi - \psi\boldsymbol{\nabla}\tilde{\psi}\right) + \psi\tilde{\psi}\left(|\psi|^2 + \left(\frac{\ell}{\lambda}\right)^2|\mathbf{A}|^2 - 1\right)\right\} d\Omega = 0$$
$$\forall\; \tilde{\psi} \in \mathcal{H}^1(\Omega) \text{ and} \tag{3.12}$$

$$\int_\Omega \left\{ \left[\frac{i}{2} \frac{\xi}{\lambda} \left(\psi^* \boldsymbol{\nabla} \psi - \psi \boldsymbol{\nabla} \psi^* \right) + \frac{\ell^2}{\lambda^2} |\psi|^2 \mathbf{A} \right] \cdot \tilde{\mathbf{A}} \right\} d\Omega$$
$$+ \int_\Omega \left[\sigma \frac{\ell^2}{\lambda^2} \frac{\partial \mathbf{A}}{\partial t} \cdot \tilde{\mathbf{A}} + (\boldsymbol{\nabla} \times \mathbf{A}) \cdot \left(\boldsymbol{\nabla} \times \tilde{\mathbf{A}} \right) + (\boldsymbol{\nabla} \cdot \mathbf{A}) \left(\boldsymbol{\nabla} \cdot \tilde{\mathbf{A}} \right) - \mathbf{H} \cdot \left(\boldsymbol{\nabla} \times \tilde{\mathbf{A}} \right) \right] d\Omega$$
$$+ \left[\frac{1}{|\Omega_0|} \int_{\Gamma_1} (\mathbf{A} \times \hat{\mathbf{n}}) \, d\Gamma_1 - \mathbf{H} \right] \cdot \left[\int_{\Gamma_1} \left(\tilde{\mathbf{A}} \times \hat{\mathbf{n}} \right) \, d\Gamma_1 \right]$$
$$+ \int_\Gamma \left[\frac{1}{\epsilon} (\mathbf{A} \cdot \hat{\mathbf{n}}) \left(\tilde{\mathbf{A}} \cdot \hat{\mathbf{n}} \right) \right] d\Gamma = 0 \; \forall \; \tilde{\mathbf{A}} \in \mathbf{H^1}(\boldsymbol{\Omega}). \tag{3.13}$$

Our simulations will be approximate numerical solutions of equations (3.12)–(3.13).

4 FINITE DIENSIONAL APPROXIMATION OF WEAK SOLUTION

Semi-discrete problem

In order to obtain a numerical approximation of equations (3.12)–(3.13), we require discretization schemes of both time and space. We use the Galerkin finite element method (FEM) in space to obtain the semi-discrete problem.

Let us start by choosing a set of points, called global nodes, in Ω and on Γ. We then obtain a Delaunay triangulation of the global nodes. If an edge is common to two triangles (the endpoints are not both on Γ), we add a node at the midpoint of the edge and do not change the boundary. Otherwise, we add the node on Γ and reshape the boundary to a quadratic curve that interpolates the three nodes on Γ. Figure 4.1 is an annulus partitioned into our isoparametric elements. For our simulations, many more global nodes were used.

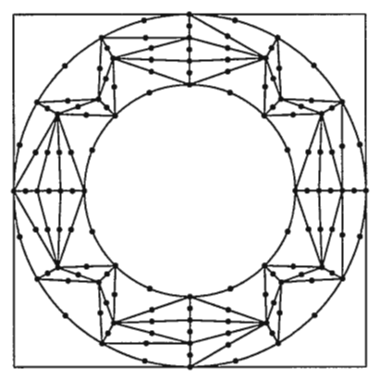

Figure 4.1 Nodes and isoparametric elements

We can now define a Lagrange finite element (K, P_K, Θ_K). $K \subseteq \mathbb{R}^2$ denotes an isoparametric element. P_K is the set of quadratic polynomials on K. An element of Θ evaluates the elements of P_K at the node values. P_K =span$\{1, x, y, x^2, y^2, xy\}$ is a finite dimensional space of real-valued functions on K. Given six function values at the nodes of K, there is a unique second-order polynomial

(element of P_K) that interpolates that data, so Θ_K is P_K-unisolvant. The set of all our finite elements, $\{(K_j, P_{K_j}, \Theta_{K_j})\}$, forms a finite element space.

Let S^h be the set piecewise quadratic polynomials on Ω. At each time step, we solve equations (3.12)–(3.13) with elements $\psi^h \in \mathcal{S}^h$ and $\mathbf{A}^h \in \mathbf{S}^h$, where

$$S^h = \{p \in C(\Omega) : p|_{K_j} \in P_{K_j} \ \forall \, \mathrm{j}\}, \tag{4.1}$$

$$\mathcal{S}^h = S^h + iS^h, \text{ and} \tag{4.2}$$

$$\mathbf{S}^h = \left[S^h\right]^2. \tag{4.3}$$

Once we have chosen bases for $\mathcal{S}^h$ and $\mathbf{S}^h$, this amounts to solving a system of non-linear equations. As we shall see, if we choose a large number of close global nodes, $\psi^h \approx \psi$ and $\mathbf{A}^h \approx \mathbf{A}$.

Let $\varphi_j \in S^h$ be the unique piecewise quadratic polynomial that is one at global node j and zero at every other global node. $\{\varphi_j\} \subseteq S^h$ forms a basis of S^h, $\mathcal{S}^h$, and $\mathbf{S}^h$ over the fields $\mathbb{R}$, $\mathbb{C}$, and $\mathbb{R}^2$ respectively. This basis, which we shall use for our calculations, offers conceptual and computational advantages. Any $\psi^h \in \mathcal{S}^h$ and $\mathbf{A}^h \in \mathbf{S}^h$ are linear combinations of their nodal values, $\left\{\psi_j^h\right\} \subseteq \mathbb{C}$ and $\left\{\mathbf{A}_j^h\right\} \subseteq \mathbb{R}^2$:

$$\psi^h = \sum_j \left(\psi_j^h \varphi_j\right) \text{ and} \tag{4.4}$$

$$\mathbf{A}^h = \sum_j \left(\mathbf{A}_j^h \varphi_j\right). \tag{4.5}$$

As we shall see, this choice of basis also reduces the amount of computation required since a basis function φ_j is zero on every element that does not have j as a local node.

Fully discrete method

To discretize in time, we use finite difference approximations of $\frac{\partial \psi}{\partial t}$ and $\frac{\partial \mathbf{A}}{\partial t}$. We combine the backward Euler method in time and the Galerkin FEM in space to obtain a fully discrete method.

Let $\psi_0(\mathbf{x})$ and $\mathbf{A}_0(\mathbf{x})$ be the initial conditions of ψ and $\mathbf{A}$, which are known. We make the approximations that, given a sequence of time steps $\{\Delta t_k\} \subseteq \mathbb{R}$, at time $t_j = \sum_{k=1}^{j} \Delta t_k$,

$$\frac{\partial \psi}{\partial t} \approx \frac{\psi_j - \psi_{j-1}}{\Delta t_j} \text{ and} \tag{4.6}$$

$$\frac{\partial \mathbf{A}}{\partial t} \approx \frac{\mathbf{A}_j - \mathbf{A}_{j-1}}{\Delta t_j}. \tag{4.7}$$

Our fully discrete problem becomes: at time $t_k = \sum_{l=1}^{k} \Delta t_l$, find $\psi_k^h = \sum_i \psi_{k,i}^h \varphi_i \in \mathcal{S}^h$ and $\mathbf{A}_k^h =$

$\sum_i \mathbf{A}^h_{k,i}\varphi_i \in \mathbf{S}^h$ such that:

$$\int_\Omega \left\{ \left(\frac{\psi^h_k - \psi^h_{k-1}}{\Delta t_k} \right) \varphi_j + \left(\frac{\xi}{\ell} \right)^2 (\boldsymbol{\nabla}\psi^h_k) \cdot (\boldsymbol{\nabla}\varphi_j) \right.$$
$$\left. + i\frac{\xi}{\lambda}\mathbf{A}^h_k \cdot (\varphi_j \boldsymbol{\nabla}\psi^h_k - \psi^h_k \boldsymbol{\nabla}\varphi_j) + \psi^h_k \varphi_j \left(\left|\psi^h_k\right|^2 + \left(\frac{\ell}{\lambda} \right)^2 \left|\mathbf{A}^h_k\right|^2 - 1 \right) \right\} d\Omega = 0 \ \forall \ \mathrm{j} \text{ and} \quad (4.8)$$

$$\int_\Omega \left\{ \left[\frac{i}{2}\frac{\xi}{\lambda} \left(\psi^{h^*}_k \boldsymbol{\nabla}\psi^h_k - \psi^h_k \boldsymbol{\nabla}\psi^{h^*}_k \right) + \frac{\ell^2}{\lambda^2} \left|\psi^h_k\right|^2 \mathbf{A}^h_k \right] \cdot (\varphi_j \hat{\mathbf{x}}_m) \right\} d\Omega$$
$$+ \int_\Omega \left\{ \sigma \frac{\ell^2}{\lambda^2} \left(\frac{\mathbf{A}_k - \mathbf{A}_{k-1}}{\Delta t_k} \right) \cdot (\varphi_j \hat{\mathbf{x}}_m) + (\boldsymbol{\nabla} \times \mathbf{A}) \cdot [\boldsymbol{\nabla} \times (\varphi_j \hat{\mathbf{x}}_m)] + (\boldsymbol{\nabla}\cdot\mathbf{A} - \mathbf{H}) [\boldsymbol{\nabla}\cdot(\varphi_\mathbf{j}\hat{\mathbf{x}}_\mathbf{m})] \right\} d\Omega$$
$$+ \left[\frac{1}{|\Omega_0|} \int_{\Gamma_1} (\mathbf{A} \times \hat{\mathbf{n}}) \, d\Gamma_1 - \mathbf{H} \right] \cdot \left[\int_{\Gamma_1} (\varphi_j \hat{\mathbf{x}}_m \times \hat{\mathbf{n}}) \, d\Gamma_1 \right]$$
$$+ \int_\Gamma \left[\frac{1}{\varepsilon} (\mathbf{A}\cdot\hat{\mathbf{n}}) (\varphi_j \hat{\mathbf{x}}_m \cdot \hat{\mathbf{n}}) \right] d\Gamma = 0 \ \forall \ \mathrm{j}, \text{ where } \hat{\mathbf{x}}_m \in \{\hat{\mathbf{x}}, \hat{\mathbf{y}}\} . \quad (4.9)$$

The backward Euler method is an implicit scheme, so at each time step t_k, we solve a system of non-linear equations to get $\left\{\psi^h_{k,i}\right\}$ and $\left\{\mathbf{A}^h_{i,k}\right\}$, the nodal values of ψ^h_k and $\mathbf{A}^h_k$ respectively. As we shall see in the next section, if h is the maximum length of the boundaries of the isoparametric elements, then as $h \to 0$, $\psi^h_k(\mathbf{x}) \to \psi(t_k, \mathbf{x})$ and $\mathbf{A}^h_k(\mathbf{x}) \to \mathbf{A}(t_k, \mathbf{x})$.

Error in Euler-Galerkin method

In developing our fully discrete method, equations (4.8)–(4.9), we made three approximations which induce error in our solution. We added the ε-penalty term to the boundary condition of $\mathbf{A}$, used the FEM to discretize space, and used the backward Euler method to discretize time.

Let h be the maximum boundary length of all our isporametric elements. At some time step t_k, the optimal H^0-error and H^1-error from the FEM will be $\mathcal{O}(h^3)$ and $\mathcal{O}(h^2)$ respectively [16]. Let $(\psi, \mathbf{A})$ be the solution of the weak formulation, and let $(\psi^h, \mathbf{A}^h)$ be the Euler-Galerkin method solution. There exist constants, $C_{k,1}$ and $C_{k,2}$, which depend on t_k, such that

$$\| \psi(t_k, \cdot) - \psi^h_k \|_0 + \| \mathbf{A}(t_k, \cdot) - \mathbf{A}^h_k \|_0 \leq C_{k,1} h^3 \text{ and} \quad (4.10)$$
$$\| \psi(t_k, \cdot) - \psi^h_k \|_1 + \| \mathbf{A}(t_k, \cdot) - \mathbf{A}^h_k \|_1 \leq C_{k,2} h^2. \quad (4.11)$$

If we choose the $\varepsilon = h^2$, then the error from the penalty method will be of the same order as the FEM method [18].

The global error from the backward Eulder method is $\mathcal{O}(\Delta t)$. The local error is $\mathcal{O}\left(C_t \Delta {t_k}^2\right)$, where C_t depends on the time, but not Δt_k. As $\frac{\partial\psi}{\partial t}, \frac{\partial\mathbf{A}}{\partial t} \to 0$, $C_t \to 0$, so for the steady state of the system,

the errors from the FEM and the penalty method will dominate the total error. The fact that C_t is small when the system in not changing much allows us to use a varying time step to reach steady state in fewer time steps. If we can determine that the system is slowly changing, then C_t will be small, so we can make Δt_k larger.

The value of h also determines the resolution of the grid. For a coarse grid (large h), the problem size and computation time are reduced, but the grid might not capture all the vortex motion. In some instances, as we decreased h, new vortices appeared. Refining the grid mesh, however, significantly increases the time required by the computers to reach the steady state of the system. To strike a balance between speed and accuracy, some experimentation is required. We keep refining the mesh until the steady state becomes stable. As we shall see in chapter 5, the number of vortices increases as H increases. A finer mesh is required to capture all of the vortices at higher H values.

Numerical solution schemes

To solve the fully discrete method, equation (4.8)–(4.9), we need a method of numerical integration, a method of solving the non-linear equations, and a method of evaluating the basis functions, $\{\varphi_j\}$, and their partial derivatives.

Numerical integration and evaluation of the basis functions are performed with the help of a reference triangle. As we can see from Figure 4.2, the reference triangle in ξ-η space is much simpler than the isoparametric element in x-y space. The midpoint quadrature rule is used on the reference triangle. The basis functions and their derivatives are also evaluated on the reference triangle. The results are then mapped to the isoparametric element using the quadratic polynomial that maps the ξ-η space to the x-y space.

At each time step, Newton's method is used to solve the system of non-linear equations. The initial

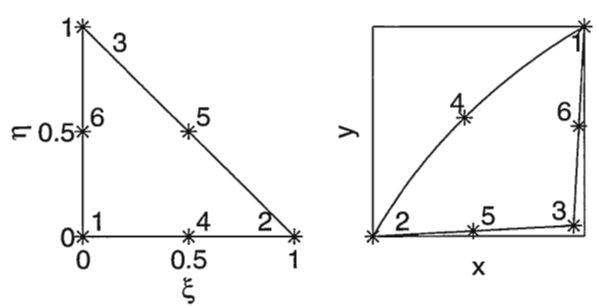

Figure 4.2 Reference Triangle and isoparametric element

guess is taken to be the solution at the previous time step. At each iteration step, the BiConjugate Gradient Stabilized (Bi-CGSTAB) iterative solver [19] is used to solve the linear system of equations. The initial guess is taken to be the solution at the previous Newton iteration.

The $J_{i,j}$ element of the Jacobian matrix, J, is a sum of terms involving the product of φ_i and φ_j or their derivatives. If global nodes i and j are on different elements, then $\text{support}(\varphi_i\varphi_j) = \emptyset$, and $J_{i,j}$ will be zero. Since J is a sparse matrix, the non-zero elements are stored in the Compressed Sparse Row (CSR) format. By adding the ε-penalty term to the boundary condition of $\mathbf{A}$ and the $\boldsymbol{\nabla}\cdot(\boldsymbol{\nabla}\mathbf{A})$ term to the Ginzburg-Landau equation, we ensure that as long as Δt_k is not too large, J is symmetric and positive definite.

A direct Cholesky decomposition solver can not be used in this case because of storage considerations. In order for a banded storage scheme to be feasible, the global node numbers of nodes on the same element must be close. If not, many zero entries of J are stored, and unnecessary computations are performed. This is not an issue with CSR storage and the Bi-CGSTAB method. Numbering our global nodes with banded storage in mind proved too difficult.

We use the convergence of Newton's method to determine our time step, Δt. If only two iterations are required, then Δt is increased. If the iterative linear solver fails to converge, then Δt is decreased.

5 NUMERICAL SIMULATIONS OF THE WEAK FORMULATION OF THE TDGL EQUATIONS

Visualization of the data

As stated in the introduction, we are interested in the behavior of the vortices in the sample. At the center of a vortex is a normal region, so $\psi = |\psi| e^{i\phi} = 0$. Using a contour plot of $|\psi|$ and a vector plot of $e^{i\phi}$, we can find the zero points of ψ.

A contour plot of $|\psi|$ gives us an indication of the locations of the vortices by showing where $|\psi|$ is small. By plotting eleven contour lines between the minimum and maximum values of ψ^h, we appear to get regions which contain normal centers. We can not be sure, however, that these points are near an actual zero of ψ. We therefore use information about ϕ. The Ginzburg-Landau model implies that the flux through any closed curve in Ω is quantized, and so ϕ must change by integral multiples of 2π on the curve [4, pages 127–128]. Counting the number of times ϕ goes around on the curve gives the number of flux quanta through the curve. If the closed curve has a vortex in it, then the flux through the curve is non-zero. As we can see in Figure 5.1, a vector plot of $\cos(\phi)\hat{\mathbf{x}} + \sin(\phi)\hat{\mathbf{y}}$ allows us to see the curves that have a zero of ψ in them and so determine whether the points where $|\psi|$ is small are actually near the center of vortex. None of the vector plots are presented since it is evident from the contour plots of $|\psi^h|$ where the vortices are. Each apparent vortex was confirmed, however, using its vector plot.

Intermediate state numerical simulations

At all times, the magnetic field, $\mathbf{h}$, in the outer normal region, Ω_2, is the same as the applied magnetic field. Initially, $\mathbf{h} = \mathbf{0}$ in the interior normal region, Ω_0. Vortices form at the exterior boundary, Γ_2, and transport flux to Ω_0. After enough vortices enter Ω_0, the remaining vortices move back into the interior of Ω where steady state is reached. As an example, we tabulate some of the intermediate states of a superconducting annulus with applied magnetic field $H = 0.6\kappa$ and inner radius $R_1 = 5.0$. In Table 5.1,

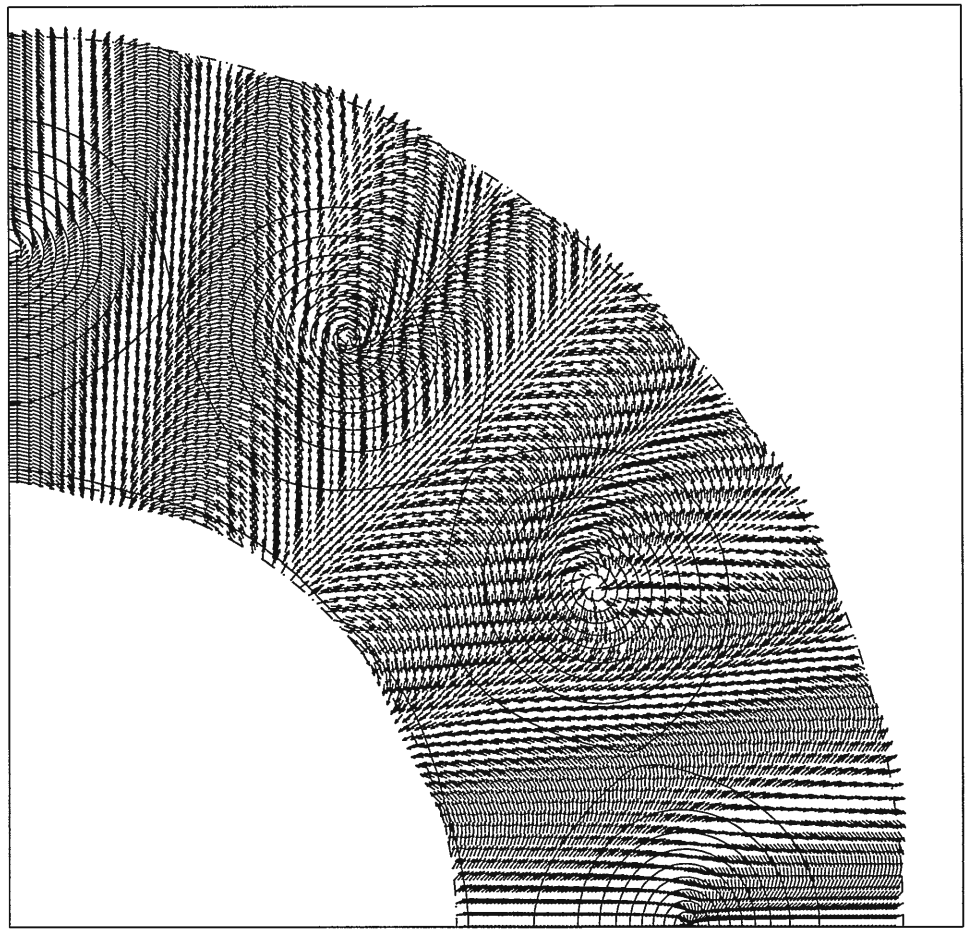

Figure 5.1 Contour plot of $|\psi|$ and vector plot of ϕ

we see twenty vortices form on Γ_2 and then move towards the inner boundary, Γ_1. After eight vortices enter Ω_0, we see in Table 5.2 that the remaining twelve vortices move into the steady state formation in the interior of Ω.

Steady state numerical simulations

We perform two sets of numerical simulations. In the first group, we hold the applied field, H, constant and vary the inner radius, R_1. We expect that for a thin enough ring, no vortices will appear. In the second group of simulations, we hold R_1 constant and vary H. If H is larger than a critical field, H_{c3}, superconductivity is lost. From the simulations, we determine how the number of vortices change as we vary R_1 and H. We also try to determine the values of R_1 and H where no vortices are present. All of the remaining results are for the steady states of the systems.

Table 5.1 Vortex transport of flux to Ω_0

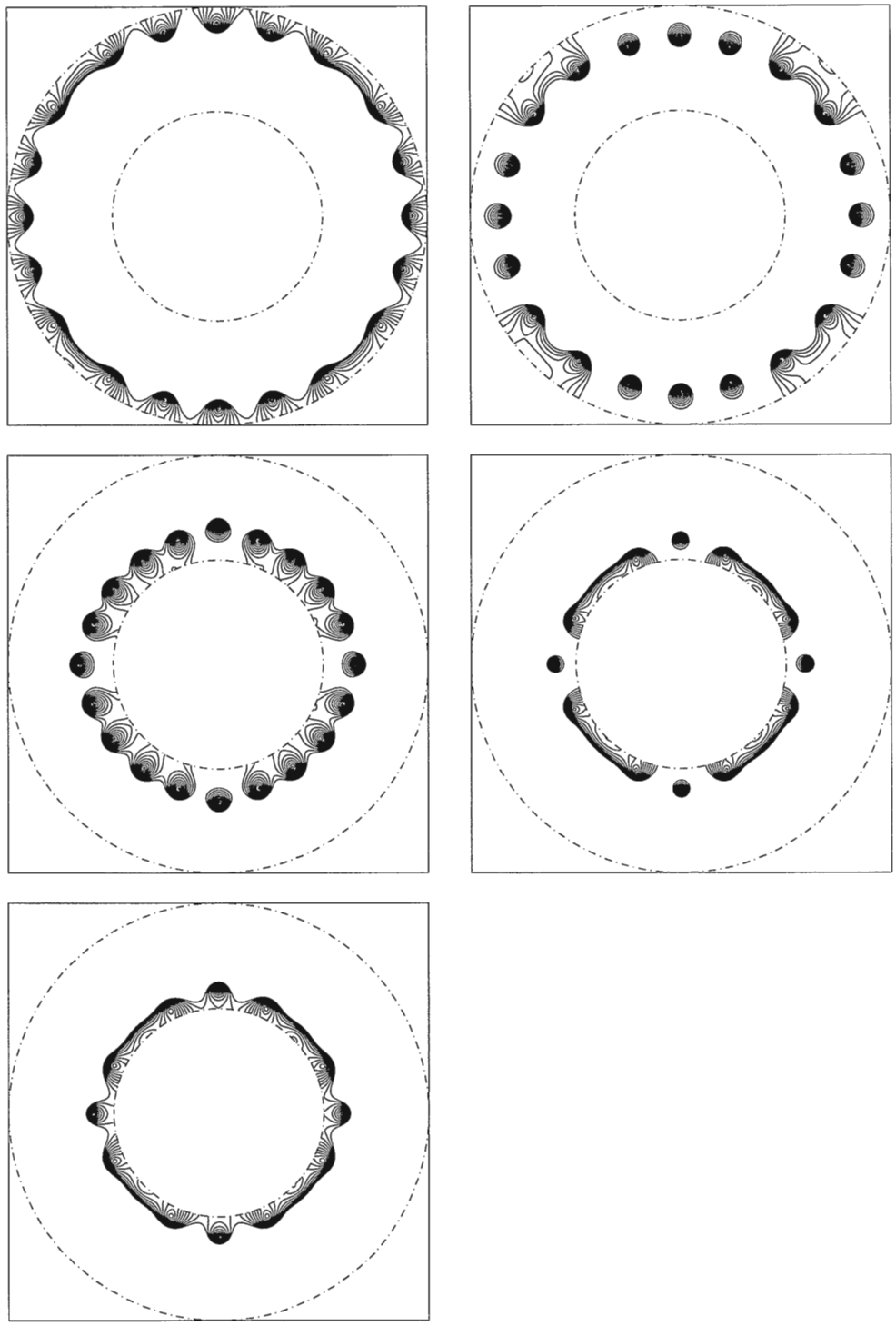

Table 5.2 Vortex movement to steady state

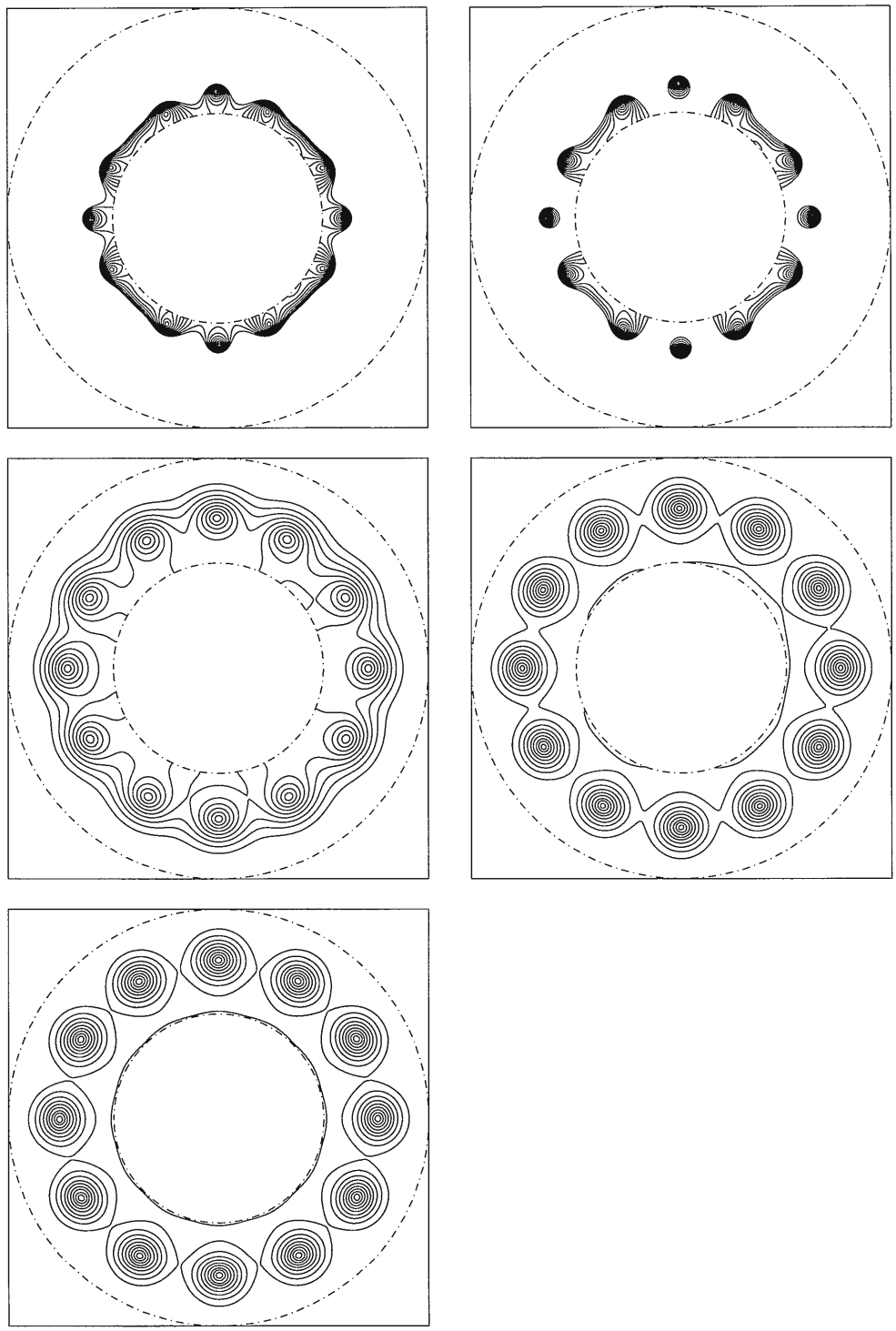

In Table 5.3, we fix $H = 0.6\kappa$ and vary R_1 from 5.0 to 6.4. The number of vortices that are present at the steady state solution are tabulated. As we can see from the table, the number of vortices starts out at 12 and then decreases as we make the ring thinner. Between $R_1 = 6.3$ and $R_2 = 6.4$, the number of vortices drops from 2 to 0. In Figures 5.3–5.5, we show how the number of vortices decrease as we increase R_1. For a larger value of H, the size of the vortices decreases so we expect vortices to form at larger values of R_1.

In Table 5.4, we fix $R_1 = 6.0$ and vary $H = 0.6\kappa$ from 0.6κ to 1.6κ. The number of vortices that are present at the steady state solution are tabulated. As we can see from the table, the number of vortices starts out at 8 and then increases as we increase H. The largest field included is $H = 1.6\kappa$, which has 34 vortices. As we can see from Figure 5.2, for larger H ($H = 1.7\kappa$ and $H = 1.8\kappa$), the maximum value of ψ^h at the nodes drops to almost zero. This is expected since, as we discussed in Chapter 1, if H is greater than a critical field, then superconductivity is lost. For a type-II superconductor with boundaries, there are three different critical fields, $H_{c1} < H_{c2} < H_{c3}$. The location of H between the three critical fields determines the behavior of the superconductor. For a weak magnetic field, $H < H_{c1}$, no flux penetrates the superconductor. For $H_{c1} < H < H_{c2}$, flux penetrates the sample, and vortices form [20, pages 48–49]. In our dimensionless system of units, the theoretical value of H_{c2} is $H_{c2} = \kappa$ [4, page 135]. If the sample has boundaries, as ours does, then superconductivity is maintained near the boundary for $H_{c2} < H < H_{c3}$. Superconductivity is completely lost for $H > H_{c3}$. In most cases, $H_{c3} \approx 1.69 H_{c2}$ [20, page 49]. The drop in $\max\{\psi^h\}$ occurs between $H = 1.6\kappa$ and $H = 1.7\kappa$, which agrees with expectations. In Figures 5.6–5.15, we show how the number of vortices increase as we increase H.

Table 5.3 Number of vortices with varying R_1

R_1	vortices
5.0	12
6.0	8
6.3	2
6.4	0

Table 5.4 Number of vortices with varying H

H	vortices
0.6κ	8
0.7κ	13
0.8κ	16
0.9κ	16
1.0κ	20
1.1κ	24
1.2κ	26
1.3κ	26
1.4κ	32
1.5κ	34

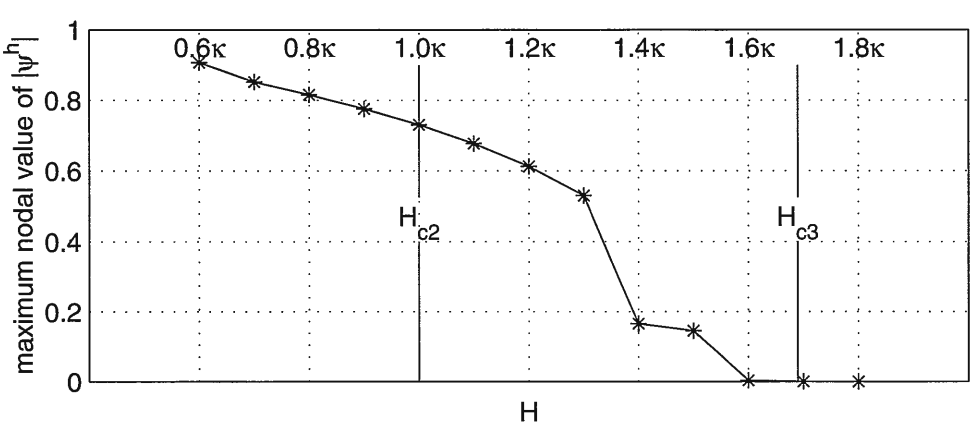

Figure 5.2 Maximum nodal value of $|\psi^h|$ versus H

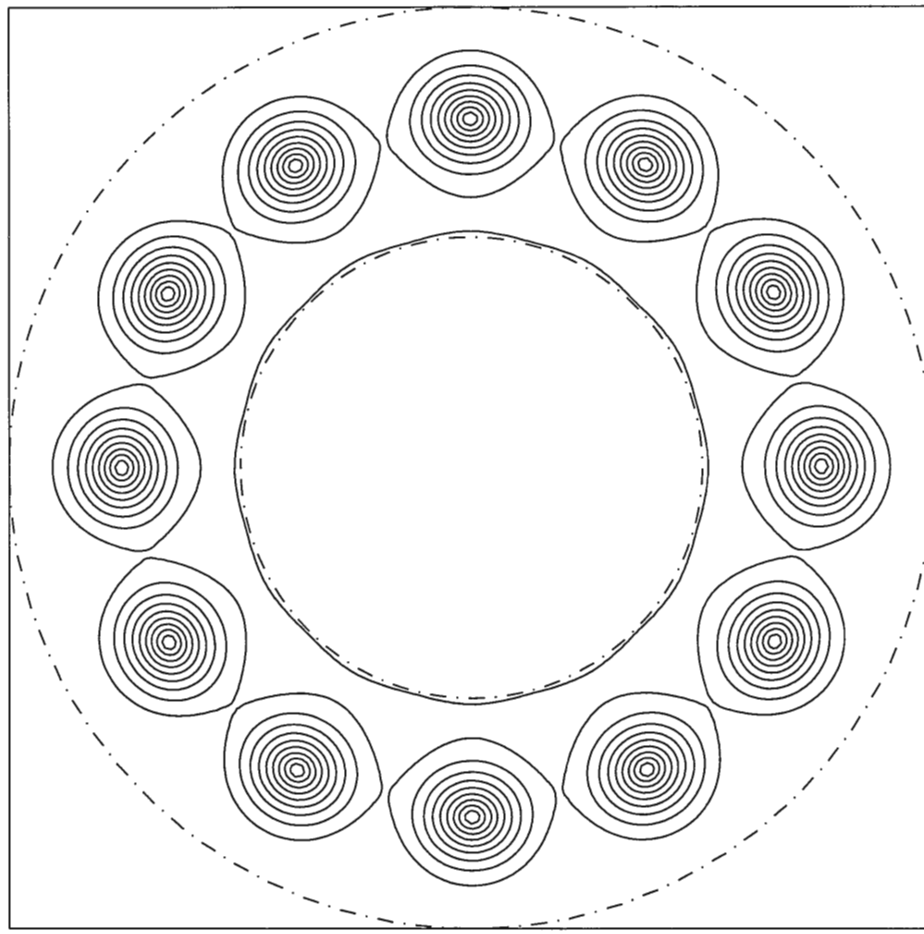

Figure 5.3 Contour plot of $\left|\psi^h\right|$ for $H = 0.60\kappa$ and $R_1 = 5.0$

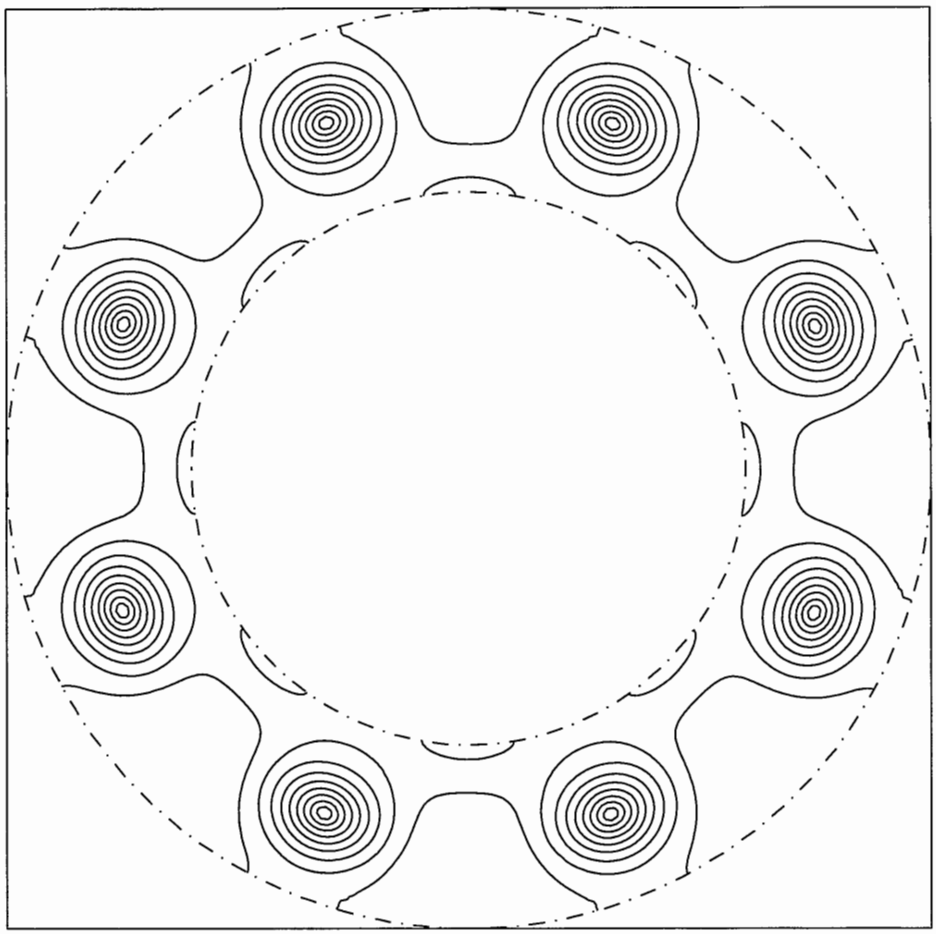

Figure 5.4 Contour plot of $\left|\psi^h\right|$ for $H = 0.60\kappa$ and $R_1 = 6.0$

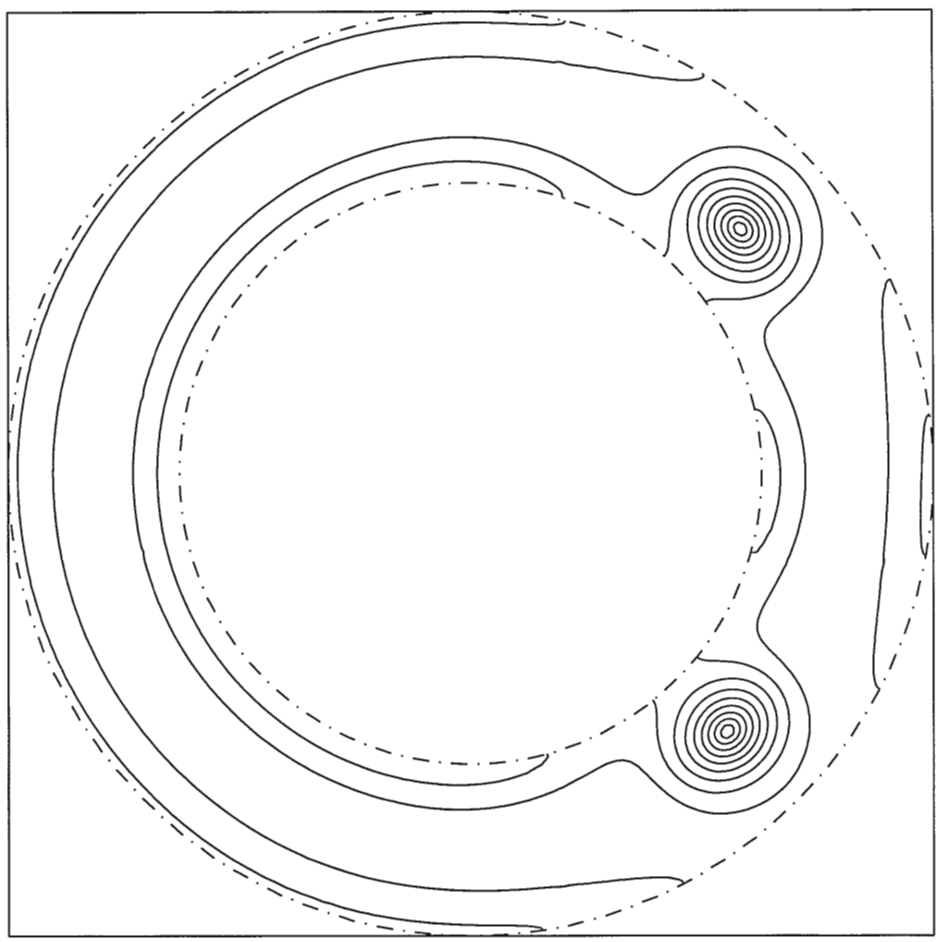

Figure 5.5 Contour plot of $\left|\psi^h\right|$ for $H = 0.60\kappa$ and $R_2 = 6.3$

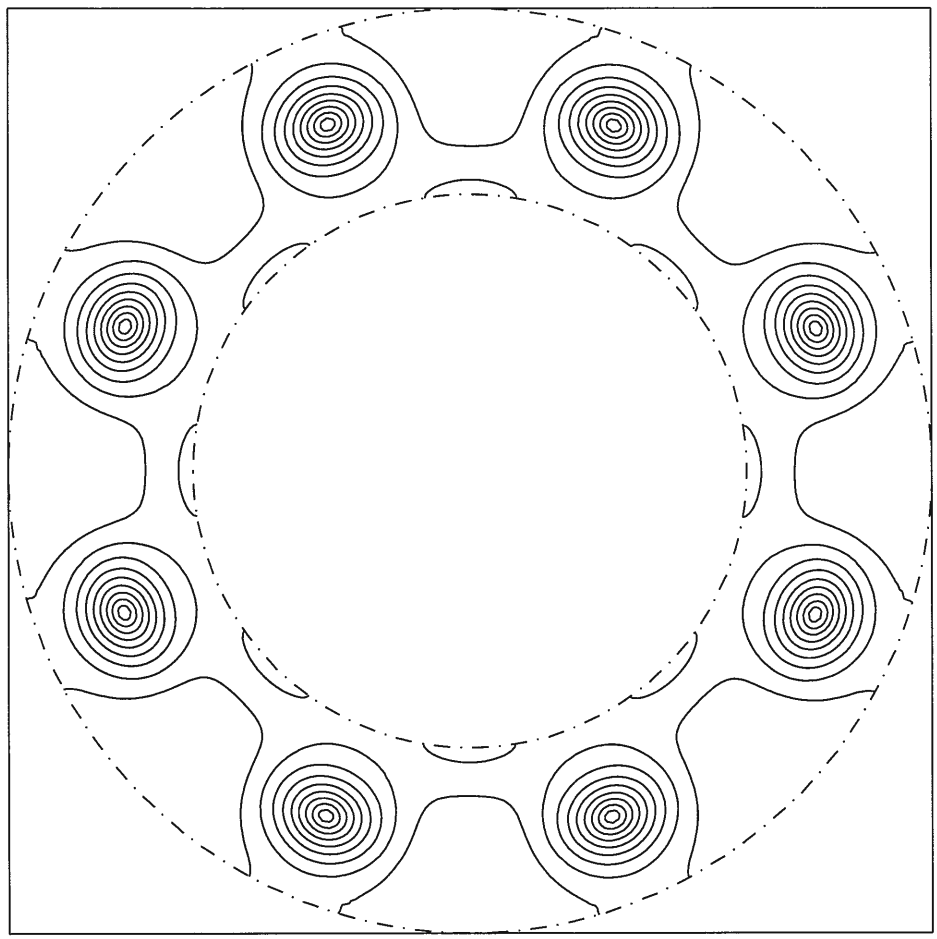

Figure 5.6 Contour plot of $\left|\psi^h\right|$ for $H = 0.60\kappa$ and $R_1 = 6.0$

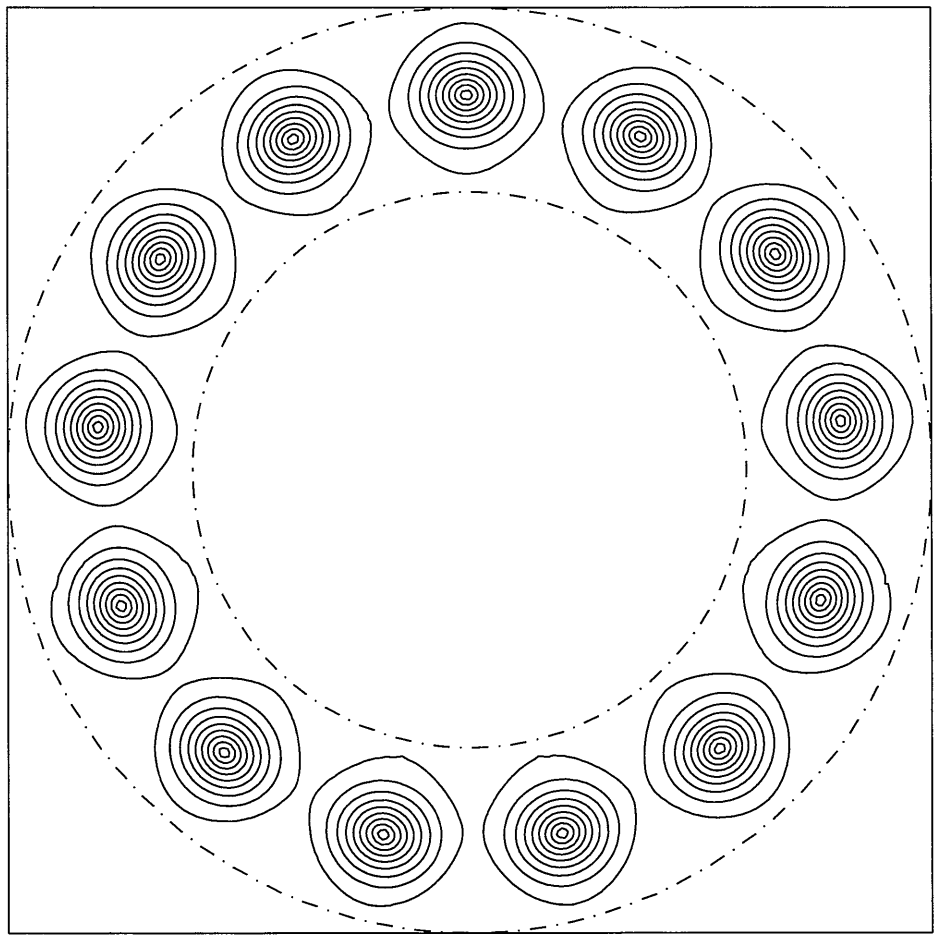

Figure 5.7 Contour plot of $\left|\psi^h\right|$ for $H = 0.70\kappa$ and $R_1 = 6.0$

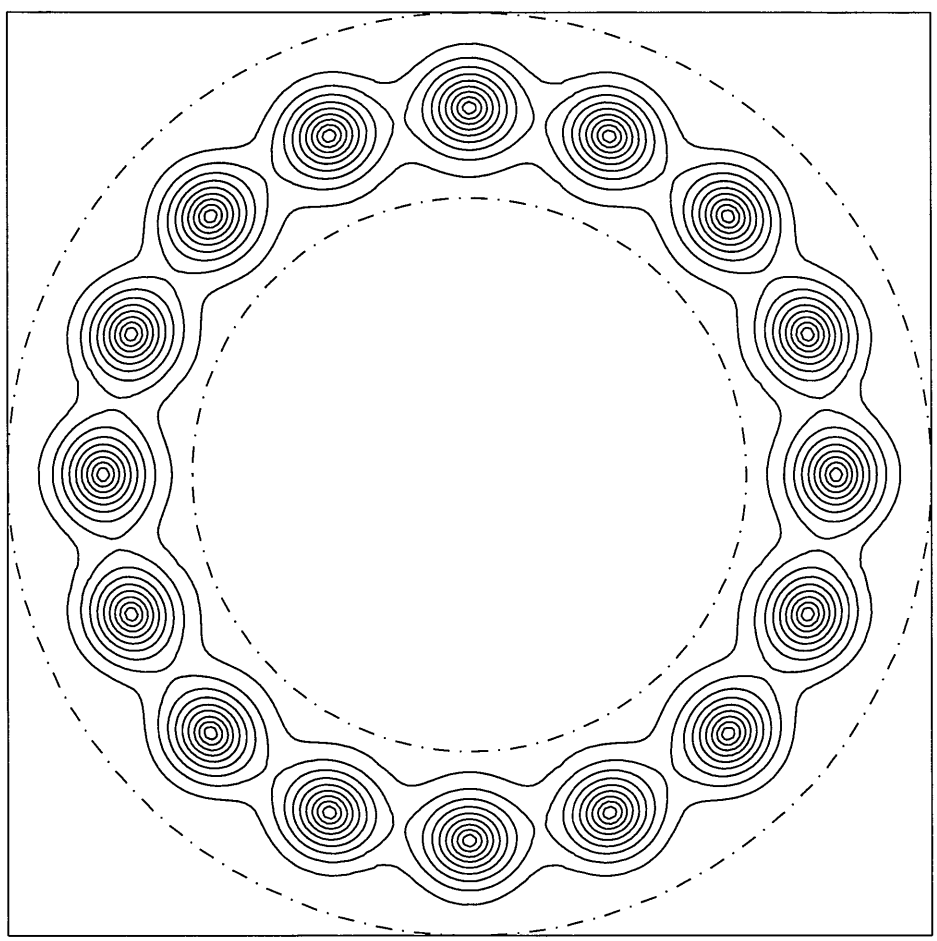

Figure 5.8 Contour plot of $\left|\psi^h\right|$ for $H = 0.80\kappa$ and $R_1 = 6.0$

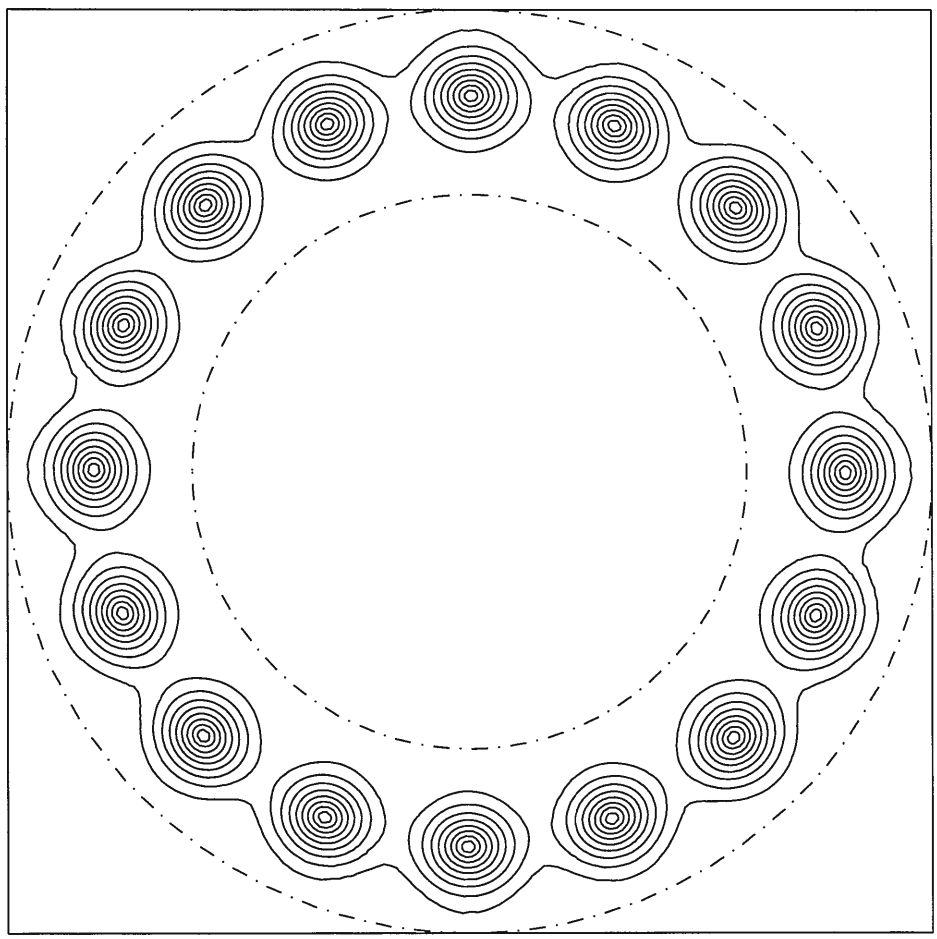

Figure 5.9 Contour plot of $\left|\psi^h\right|$ for $H = 0.90\kappa$ and $R_1 = 6.0$

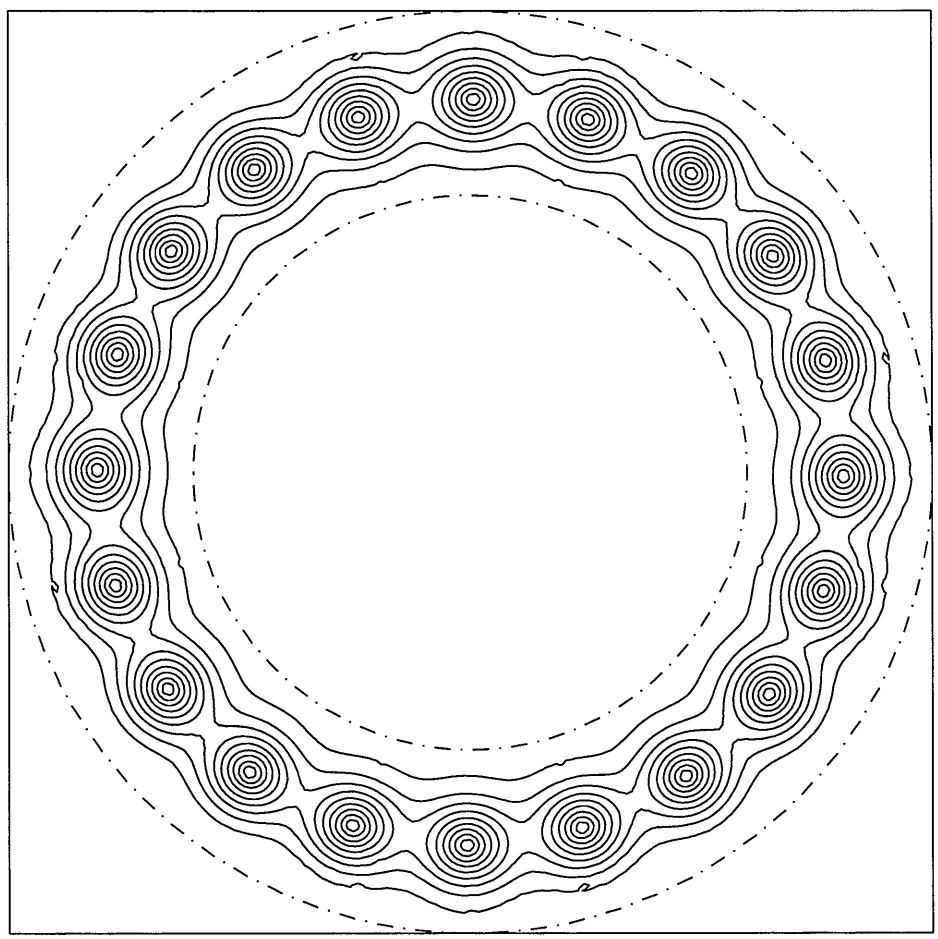

Figure 5.10 Contour plot of $\left|\psi^h\right|$ for $H = 1.00\kappa$ and $R_1 = 6.0$

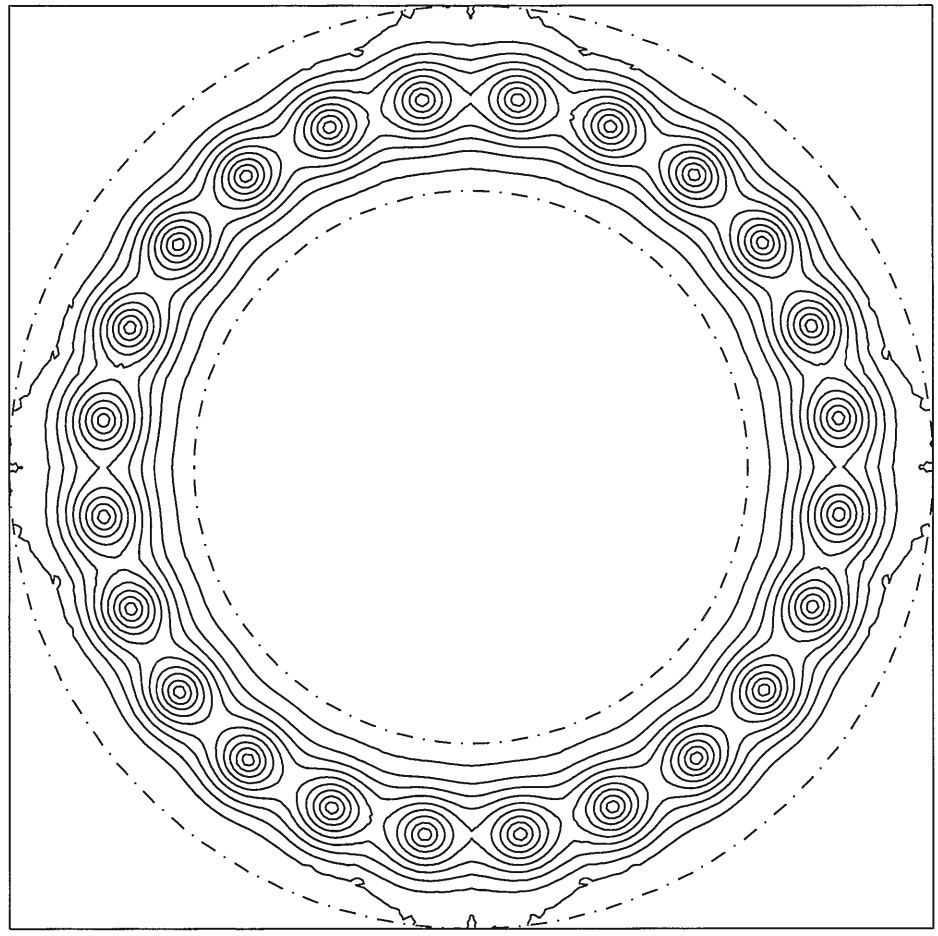

Figure 5.11 Contour plot of $\left|\psi^h\right|$ for $H = 1.10\kappa$ and $R_1 = 6.0$

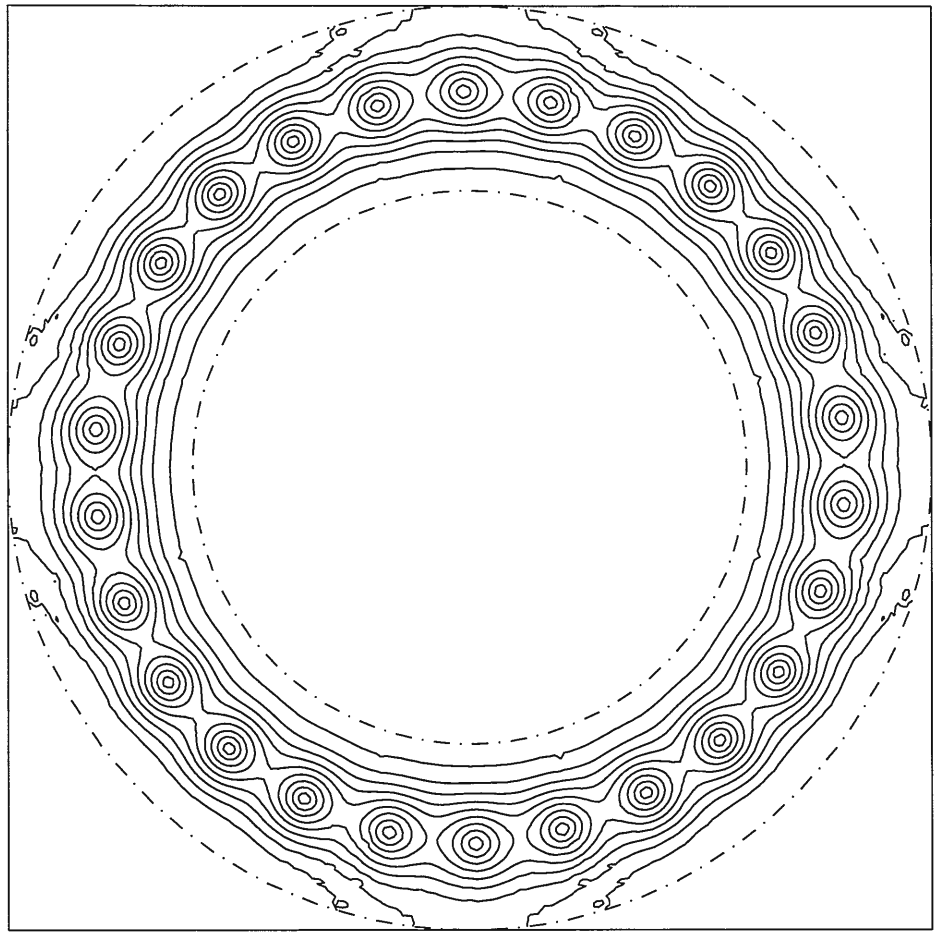

Figure 5.12 Contour plot of $\left|\psi^h\right|$ for $H = 1.20\kappa$ and $R_1 = 6.0$

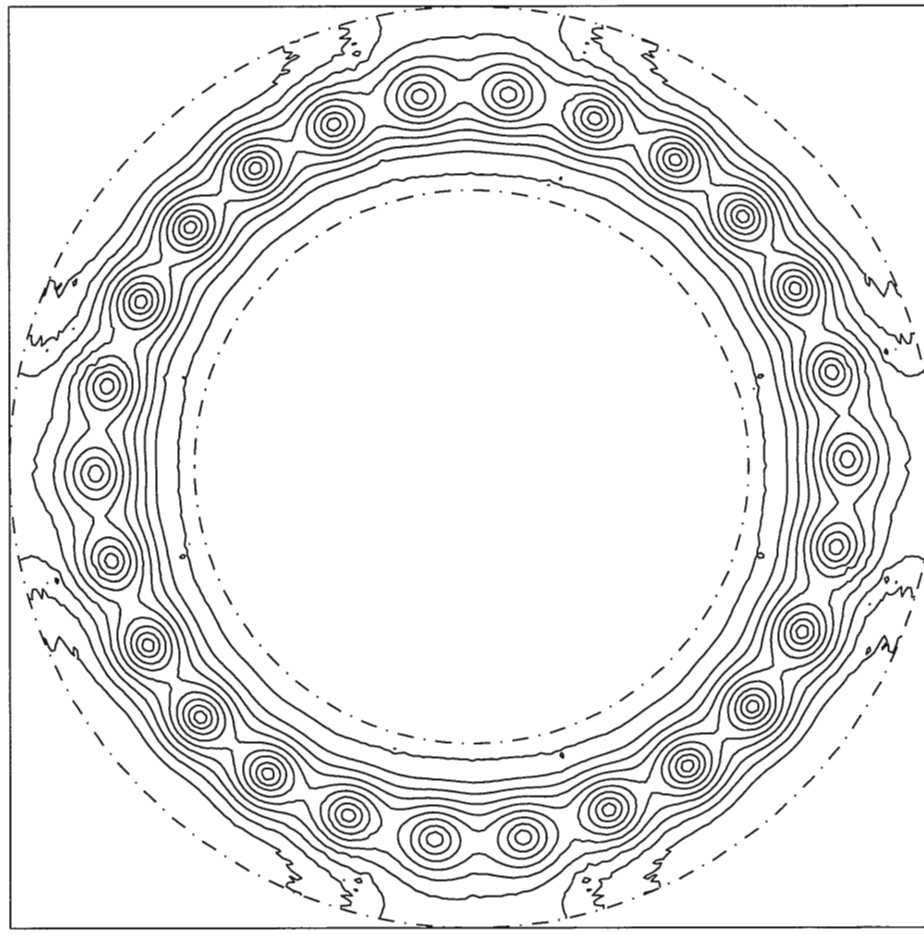

Figure 5.13 Contour plot of $\left|\psi^h\right|$ for $H = 1.30\kappa$ and $R_1 = 6.0$

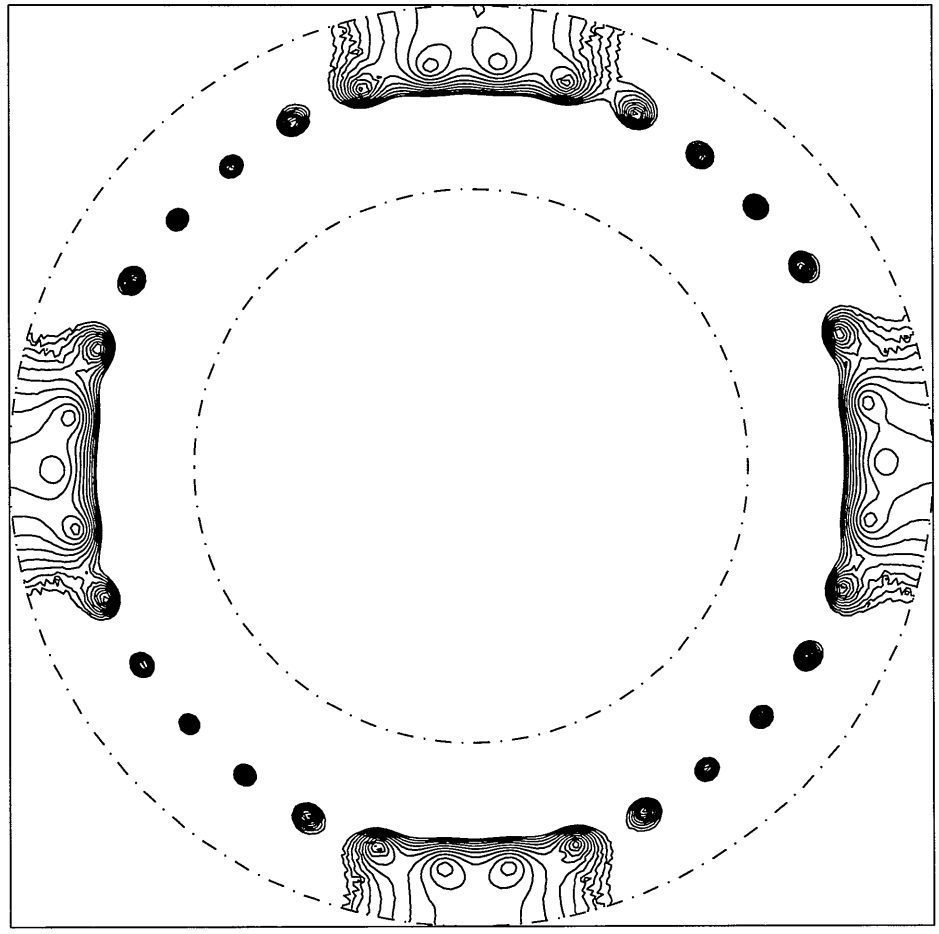

Figure 5.14 Contour plot of $\left|\psi^h\right|$ for $H = 1.40\kappa$ and $R_1 = 6.0$

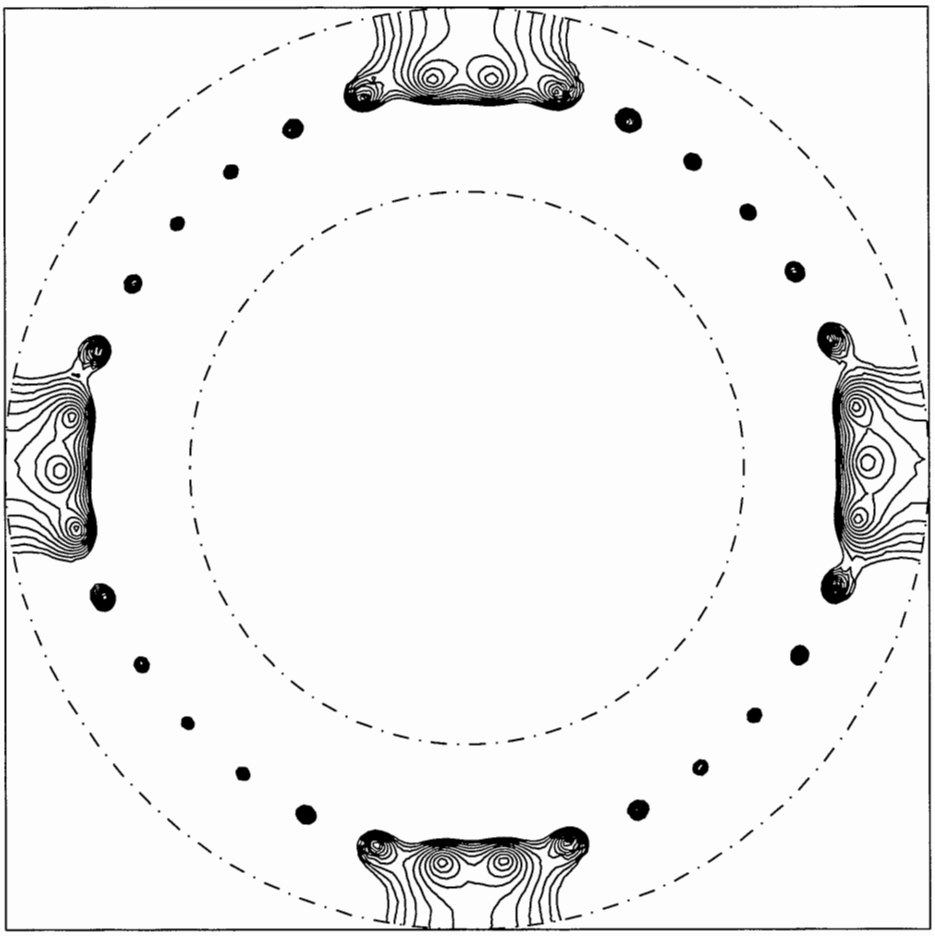

Figure 5.15 Contour plot of $\left|\psi^h\right|$ for $H = 1.50\kappa$ and $R_1 = 6.0$

BIBLIOGRAPHY

[1] B. Schechter, *The Path of No Resistance*, Simon and Schuster, New York, 1989.

[2] P. F. Dahl, *Superconductivity: Its Historical Roots and Development from Mercury to The Ceramic Oxides*, American Institute of Physics, New York, 1992.

[3] J. R. Waldram, *Superconductivity of Metals and Cuprates*, Institute of Physics Publishing, London, 1996.

[4] M. Tinkham, *Introduction to Superconductivity, Second Edition*, McGraw-Hill, New York, 1996.

[5] L. Gor'kov and N. Kopnin, *Vortex motion and resistivity of type-II superconductors in a magnetic field*, Soviet Phys. -Usp, 18 (1976), pp. 328–334.

[6] S. J. Chapman, Q. Du, and M. Gunzburger, *A Ginzburg-Landau type model of superconducting/normal junctions including Josephson junctions*, Euro. Jnl of Applied Mathematics, 6 (1995), pp. 97–114.

[7] J. D. Jackson, *Classical Electrodynamics, Third Edition*, John Wiley & Sons, New York, 1999.

[8] G. Vidali, *Superconductivity: The Next Revolution?*, Cambridge University Press, Cambridge, 1993.

[9] K. Chang, *Juggling Buckyballs Raises Hope of Warmer Superconductor*, New York Times on the Web: `http://www.nytimes.com/`, December 5, 2000.

[10] K. Chang, *Physicists Thrill to Finding of Superconductor*, New York Times on the Web: `http://www.nytimes.com/`, February 24, 2001.

[11] K. Chang, *Bell Labs' Researchers Create Plastic Superconductor*, New York Times on the Web: `http://www.nytimes.com/`, March 8, 2001.

[12] B. J. Feder, *Technology Briefing: Hardware; Utility Superconductors*, New York Times on the Web: `http://www.nytimes.com/`, July 27, 2000.

[13] B. J. Feder, *Technology Briefing: Research; Superconducting Naval Motors*, New York Times on the Web: `http://www.nytimes.com/`, November 30, 2000.

[14] G. Johnson, *Computing, One Atom at a Time*, New York Times on the Web: `http://www.nytimes.com/`, March 27, 2001.

[15] V. L. Ginzburg and E. A. Andryushin, *Superconductivity*, World Scientific, New Jersey, 1994.

[16] Q. Du, M. Gunzburger, and J. Peterson *Analysis and Approximation of the Ginzburg-Landau Model of Superconductivity*, SIAM Review, 34 (1992), pp. 54–81.

[17] Q. Du, *Global Existence and Uniqueness of Solutions of the Time-Dependent Ginzburg-Landau Model for Superconductivity*, Applicable Anal., 52 (1994), pp. 119–133.

[18] J. T. King, *New Error Bounds for the Penalty Method and Extrapolation*, Numer. Math., 23 (1974), pp. 153–165.

[19] R. Barrett, M. Berry, T. F. Chan, J. Demmel, J. Donato, J. Dongarra, V. Eijkhout, R. Pozo, C. Romine, and H. Van der Vorst, *Templates of the Solution of Linear Systems: Building Blocks for Iterative Methods*, SIAM, Philadelphia, 1994.

[20] P. G. De Gennes, *Superconductivity of Metals and Alloys.* Perseus Books, Reading, 1999.

[21] Q. Du, M. D. Gunzburger, and J. Peterson, *Solving the Ginzburg-Landau equation by finite-element methods*, Physical Review B, 46,14 (1992), pp. 9027–9034.